Arabian Journal for Science and Engineering
https://doi.org/10.1007/s13369-025-10791-w

RESEARCH ARTICLE-EARTH SCIENCES

Geochemical Evidence of the Lateritic Bauxite Deposits in the Sücüllü-Yalvaç Region (NE Isparta Angle, Southwestern Türkiye) with Emphasis on a Basic Source

Oya Cengiz[1] · M. Selman Aydoğan[2] · Betül Çoşkun Önal[3]

Received: 29 June 2025 / Accepted: 23 October 2025

Abstract

The Sücüllü (Yalvaç-Isparta, SW Türkiye) lateritic bauxite horizon lies directly on the alkali basaltic lavas (e.g. doleritic basalt) occurring on the carbonate platform of Jurassic age. This horizon is associated with thickness in the range of 5–30 m (average of 15 m) in the NW–SE direction. Lateritic bauxite occurrences have dominant mineral assemblages of clay (kaolinite, smectite), Fe-oxy-hydroxides (hematite, goethite), Al-rich minerals (boehmite, gibbsite), feldspar, cristobalite, anatase, quartz, calcite and dolomite. From bottom to top, lateritic profile is divided into 4 zones as (1) weathered basaltic rock, (2) clayey laterite zone, (3) ferrigenous laterite zone, (4) bauxite zone. Geochemically, lateritic bauxites have average values of 26.04 wt% Al_2O_3, 19.77 wt% Fe_2O_3 and 29.48 wt% SiO_2. Chemical analyses of whole rock samples and the mineral assemblage suggest that coexisting minerals of lateritic bauxite are highly aluminous and ferrigenous. Laterite and bauxite zones are typical with weak-to-moderate lateritisation. High CIA values (~ 85.7), IOL values (up to 89.62), strong depletion of major elements (Si, Mg, Ca, Na, K) and concentration of immobile elements such as Ti, Cr, Zr, Ga and REEs reflect that the studied samples can be classified as lateritic bauxite, and formed through intense chemical weathering of alkali basalt parent rocks, similar to the Payas and Çarıksaraylar bauxites in southern Taurides (Türkiye), and in the Darai-Daldali region of India. In respect of tectonic setting, these lateritic bauxites occurred under hot-humid tropical climate dominated during upper Cretaceous. Afterwards, formed lateritic bauxite materials were transported into the sea on dolomitic limestones with erosion from a terrestrial environment, and thin-bedded dolomitic limestones were deposited again on these transported laterites in the marine environment.

Keywords Lateritic bauxite · Clay · Alkali basalt · Sücüllü · Tauride · Türkiye

1 Introduction

Bauxite was defined by Berthier [1] as a rock consisting mainly of Al oxyhydroxides (gibbsite, boehmite) and Fe oxyhydroxides (goethite, hematite) and has long been a subject of study worldwide both for its importance in global industry due to its being the only source for exploitable alumina [2], other metal contents (Ga, Sc, Nb, REY) and the understanding of elemental mobility in chemical weathering of underlying bedrock lithology [3]. It is a residual rock comprising mixture of aluminium oxide minerals (diaspore, α-AlOOH; boehmite, γ-AlOOH), clay minerals (kaolinite, illite) and iron oxide minerals (hematite) occurring mostly in humid tropical to subtropical climates, in conditions where precipitation exceeds 1,2 m and the mean annual temperature is above 22 °C in particular periods of their geological history [3–7]. Based on the lithology of the underlying rock, bauxite is divided into two main categories: karstic and lateritic types [8–15]. Bauxite that lies on aluminosilicate rocks is termed laterite bauxite, and that lies on carbonate rocks is known as karst bauxite [10, 11, 3, 8, 12, 16–18]. Their ore minerals comprise several forms of gibbsite, boehmite and diaspore (hydrated aluminium oxide) [19, 20]. Of these minerals, gibbsite dominates in lateritic bauxite, whereas boehmite and diaspore are the most abundant minerals in karstic bauxite

✉ M. Selman Aydoğan
aydogan@balikesir.edu.tr

[1] Department of Geological Engineering, Süleyman Demirel University, Isparta, Türkiye

[2] Department of Geological Engineering, Balıkesir University, Balıkesir, Türkiye

[3] Department of Geological Engineering, Fırat University, Elazığ, Türkiye

Published online: 05 November 2025

[13, 14, 3, 15, 21, 22]. In addition, a mixture of goethite, hematite, kaolinite, illite and pyrophyllite and a small amount of anatase are also found in a typical bauxite rock [3, 23].

The Tauride belt has been the focus of much research because of its special tectonic and geological characteristics and various metallic and non-metallic mineral deposits such as Al, Cr, carbonate-hosted Pb–Zn deposits, sedimentary and hydrothermal barite deposits, commercial marble areas [24–31] and references therein. In land, bauxite deposits consist mainly of alumina, iron and rare earth minerals. Recently, red mud (bauxite residue), a waste by-product from the refinery during the exploitation of bauxite ores in aluminium production, has been found to contain significant concentrations of rare earth elements such as Sc, Y, La, Ce, Nd and Sm [32, 33]. ETI Aluminium in the Seydişehir region has the capacity to produce around 260,000 tonnes of red mud [34].

The Tethyan lateritisation regime of the Late Cretaceous encompasses extensive bauxite deposits in composite terranes from south-eastern France to Iran, including the Mediterranean region along the Alpine-Himalayan orogenic belt. It has long been recognised that the climate during this period was warm and humid compared to today. Many Al-rich rocks on land were lateritised to form bauxite deposits in a hot and humid tropical climate. The most important karst bauxites, known Fe-Ti bauxites and lateritic bauxite horizons of different ages and formation types, are hosted in the Tauride belt of Anatolia [30, 35]. E-W trending bauxite horizons in this belt can be considered as the eastern extension of the Alpin bauxite deposits ([36], Fig. 1A). The stratigraphic position of the giant bauxite deposits is preserved from the Tauride belt in Turkey to Iran [16, 37, 38]. This belt is generally documented as representing of a continental fragment that had rifted from a part of northern Africa called Gondwana during the Triassic period [39–42]. The bauxite deposits along Tauride belt are non-metamorphosed diasporitic and metamorphosed bauxitic Selçuk-Yatağan (Muğla), Ulubey (Uşak), Akhisar (Manisa) and diasporitic (Milas, Muğla), (Mihalıççık, Eskişehir) and mostly diasporitic Ti-rich bauxite Payas-Islahiye (Hatay), Fe-rich lateritic bauxite Sarkikaraağaç-Yalvaç (Isparta), boehmitic bauxite Seydişehir-Akseki (Konya), boehmitic–diasporitic bauxite (Bolkardağı, Karaman), diasporitic bauxite (Alanya, Antalya), boehmitic bauxite (Anamur, Mersin), diasporitic and boehmitic bauxite (Tufanbeyli-Saimbeyli-Kadirli, Adana) and boehmitic bauxite (Kokaksu, Zonguldak) in the İstanbul zone of northern Turkey ([36], Fig. 1A). Karstic bauxite deposits in the Tauride Anatolide platform and the Menderes metamorphic massif further west have been the subject of numerous studies [27, 43–51]. There have been relatively few studies of lateritic bauxite deposits in the northern part of the Isparta region and its surrounding area. Among these studies, Bozkır [52] stated that formation of lateritic bauxites between Çarıksaraylar and Kozluçay (Şarkikaraağaç, Isparta) regions occurred under the tropical climatic conditions of the Late Jurassic time. According to Coşkun [53], the terrestrial conditions formed after the shallow lagoon environment in the Late Jurassic, which were transformed from basic rocks, provided a favourable environment for the lateritisation process. The bauxites in the Yalvaç-Şarkikaraağaç region (Isparta) were formed on lateritised mafic volcanic rocks (dolerite-basalt) of Jurassic age [25, 30, 54]. These comprehensive studies have made an important contribution to the understanding of the origin of the bauxite deposits occurred in the Tauride and Anatolian continents, and in the Tethyan Metallogenic Belt.

Here, we conducted a geological, mineralogical and geochemical data of the Sücüllü lateritic bauxite deposit of the Tauride belt in eastern Mediterranean region to gain insight into its formation history. These data will contribute to the geochemical and geological knowledge of lateritic bauxite deposits derived from basaltic precursors.

2 Geological Setting

The eastern Mediterranean is characterised as a tectonically active region between the Afro-Arabian and Eurasian plates, exhibiting a wide variety of tectonic processes in a relatively small area [55]. In this terrane, a stack of interbedded allochthonous nappes forms the Taurid orogenic belt with autochthonous basement series [56–66]. Autochthonous basement rock units of the Tauride region are represented by Sultandağ (Sultandede) and Seydişehir metamorphic lithologies. In the Tauride region, allochthonous ocean-derived series can be divided into two main systems, i.e. the Antalya nappes (derived from southern Neotethys) to the south and the Lycian and Hoyran-Beysehir-Hadim nappes (derived from northern Neotethys) to the north of the continental blocks, which were rifted away from the northern margin of the Gondwana plate in the Late Permian and Early Triassic [67–72]. These nappe systems converged towards the continental blocks onto which they were thrust. Among these, Mesozoic-Paleogene carbonate and clastic sediments underlie the Hoyran-Beysehir-Hadim nappes (Fig. 1B). Both autochthonous and allochthonous series are unconformably overlain by Mesozoic to Lower Tertiary carbonate and pelagic flysch-type clastic sedimentary rocks in the eastern part of the Isparta region (Geyikdağ unit of Özgül [56]). Allochthonous units consist mainly of ophiolitic melange, sub-ophiolitic metamorphic rocks in the Şarkikaraağaç region (eastern Isparta) [73, 74].

The area of known as the Isparta Angle in SW Anatolia is one of the best known complex regions in western part of the Tauride orogenic belt. This area consists of metamorphic basement units, ophiolitic remnants (Beyşehir-Hoyran-Hadım Nappes), thick-bedded platform-type and flysch-type

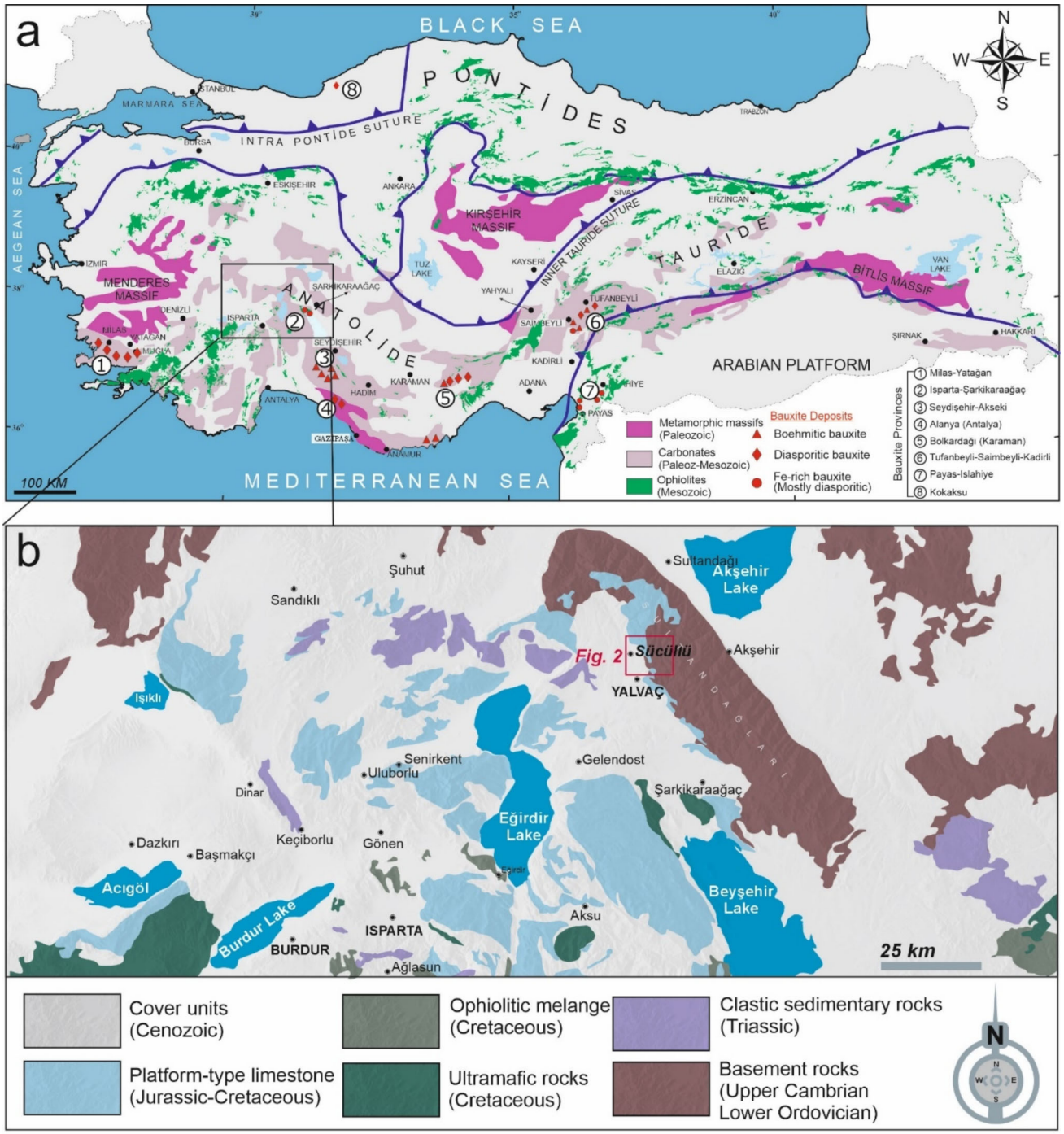

Fig. 1 **a** The main bauxite deposits and major tectonic elements and suture zones of Türkiye and the location of the Sücüllü lateritic bauxites [30, 31]. **b** Geological sketch map of the Isparta Angle, showing stratigraphical units [79, 130]

clastic carbonates and sedimentary and volcanic units of Plio-Miocene age (Fig. 2A) and has played an important role in understanding the palaeotectonic evolution of the eastern Mediterranean region [75]. This complex area was first defined by Blumental [76], and its origin was later the subject of a study by Dumont [77]. In tectonic terms, it is a palaeotectonic structure resulting from the northward curvature of the ~ NW–SE Taurid belt caused by clockwise and anticlockwise rotation in the Late Palaeocene-Early Messinian [78–81].

The Sücüllü region is located in the north-eastern corner of the Isparta Angle (Figs. 1A, 2A). In this area, the mid-Cambrian Çaltepe Limestones are the oldest lithostratigraphic unit of the sedimentary succession of the region (Fig. 2A, B; [76, 82, 83]. Its thickness is about 150 m.

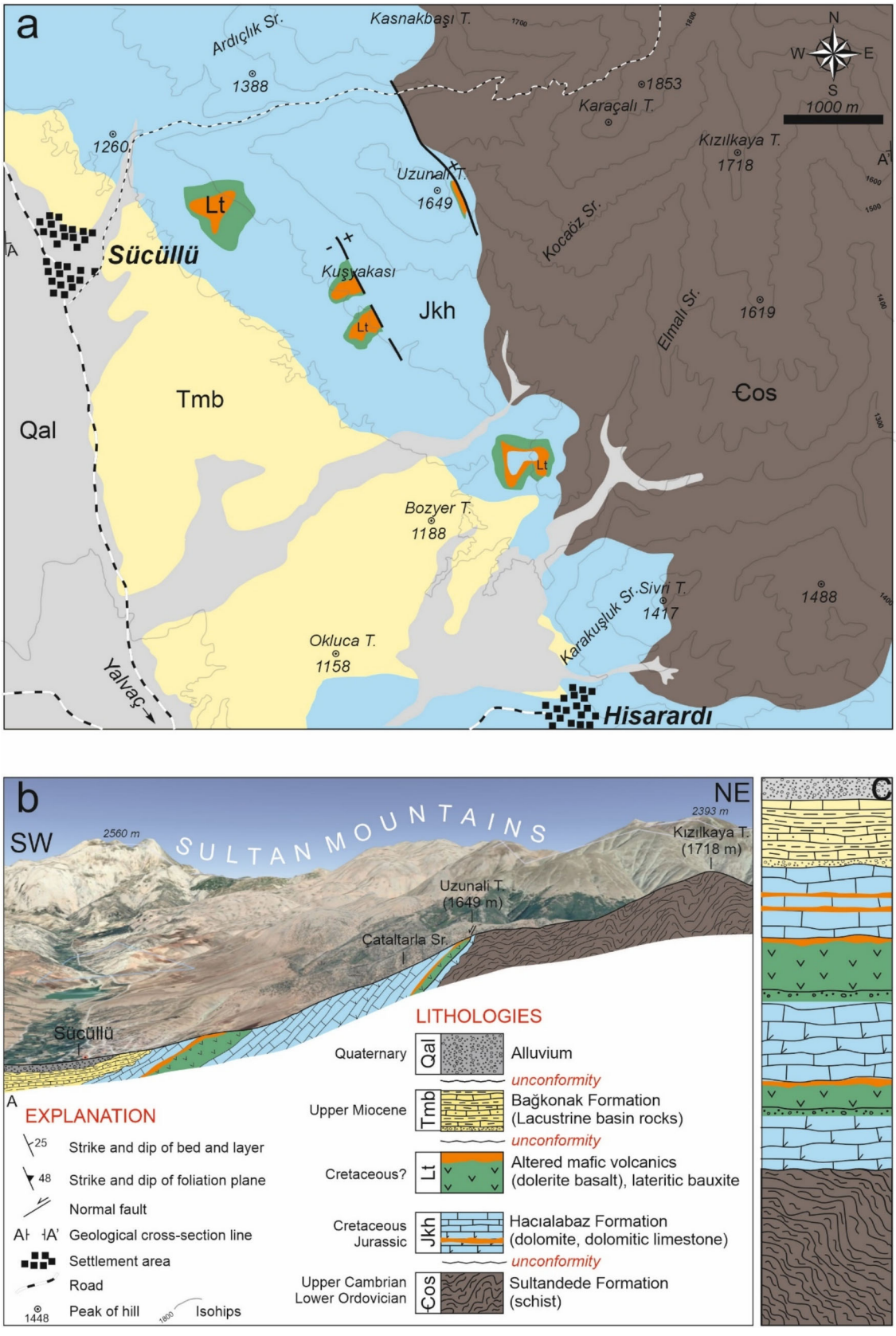

Fig. 2 **a** Geological map, **b** cross section, **c** lithostratigraphic columnar section of the Sücüllü (Yalvaç, Isparta) region

This unit consists mainly of dolomite, recrystallised limestone and nodular limestone [84]. The Çaltepe limestone gradually passes into the overlying Sultandede Formation of Upper Cambrian-Lower Ordovician age. Both units are host to a number of industrial barite deposits in the region [26, 85]. In the study area, the Sultandede Formation, composed mainly of alternations of metamorphosed sandstone, siltstone, shale and slate, forms the lower part of the stratigraphic section of the region, and it has also been observed along the Sultan Mountains in a northwest–southeast direction (Fig. 2A, B). It has been the subject of folding by the orogenic phases of the Caledonian Orogeny [26, 83, 86]. The thickness of the Sultandede Formation is in excess of 1000 m and the lower contact of this formation is not exposed in the study area. This unit is unformably overlain by the Upper Jurassic Hacıalabaz dolomitic limestone. The dolomitic carbonates are typical of a shelf environment and contain a rich benthic foraminiferal fauna. According to Turan [87], the faunas found in the Hacıalabaz limestone and the petrographical signatures of the unit indicate a low-energy, shallow and warm marine environment. The presence of dolomites supports the possibility that the depositional environment was a very shallow and lagoonal sea. This unit is intruded by submarine mafic volcanic rock (so-called Kocakızıl dolerite) and is often scattered over the outcrop of dolomitic limestone. This doleritic volcanic rocks host to numerous lateritised bauxite horizons. Hacıalabaz limestone is overlain by the Upper Miocene Bağkonak Formation, which consists mainly of sandstones, mudstones, siltstones, marls and clayey and plaquette limestones (Fig. 2A–C).

3 Material and Methods

During field trips from June–March 2010 to August 2011, we remapped Sücüllü area and lateritic bauxite samples were collected from this area. The mineralogical assemblages and geographical coordinates of the sampling sites are given in Table 1. The investigated lateritic bauxite samples (from SL-2 to S-13) were collected along the profile of the lateritic bauxite horizon from bottom to top. Weathered profile samples were collected to investigate the effects of weathering on the chemistry of the studied lateritic bauxites from bottom to top.

Based on the geochemical composition and quantities of constituent minerals, the lateritic bauxite horizon comprises four distinct stratigraphic zones that can be distinguished from bottom to top: (1) weathered mafic basalt (SL-1), (2) clayey laterite zone (SL-2 to SL-4), (3) ferruginous laterite zone (SL-5 to SL-12) and bauxite zone (SL-13) (see Fig. 6 for detail). It should be noted that since alkali doleritic basalt in the study area is mostly highly weathered, therefore, the Hawaiian alkali basalt sample (BHVO-2) provided by USGS was used as a standard reference sample for normalisation (Table 1).

X-ray powder diffraction (XRD) analyses were performed using a Rigaku Geiger Flex diffractometer with a Cu-Ka radiation anode and Ni filtration operating at a generator voltage of 40 kV and a current of 40 mA; 2θ scans varied from 2° to 72° 2-theta. Lateritic bauxite and soil samples for analysis were ground to less than 100 μm. These analyses were carried out at the Afyon Kocatepe University Laboratories (Afyonkarahisar, Turkey). Thin sections of some rock samples were examined under the Olympus (BH-2) polarizan microscope at Suleyman Demirel University.

Morphology and microchemical analyses were performed using a JEOL-6400 scanning electron microscope (SEM). Prior to SEM analysis, freshly crushed bauxite samples were attached to an aluminium substrate using carbon adhesive, coated with carbon. The scanning speed for all samples was 2°/min. The bulk mineralogy was studied with random powders. After dispersing the samples in deionised water, the < 2 mm size fraction was separated by sedimentation. Excess water was removed by centrifugation. Oriented samples were prepared from the clay fraction on glass slides.

A total of 16 ore samples were selected using a binocular microscope for geochemical analysis, which was performed at ACME Laboratories (Vancouver, Canada). Samples were crushed to less than 700 mesh for chemical analysis. The major oxides (SiO_2, TiO_2, Al_2O_3, MnO, MgO, CaO, K_2O, Na_2O, P_2O_5) and LOI of the samples were analysed by inductively coupled plasma atomic emission spectrometry (ICP-AES) after lithium metaborate/tetraborate fusion following dilute nitric acid digestion. Trace elements were analysed by inductively coupled plasma-mass spectrometry (ICP-MS), with rare earth and incompatible elements determined by $LiBO_2$ fusion and precious and base metals by aqua regia digestion. After ignition at 1000 °C, the loss-on-ignition (LOI) is the difference in weight. The detection limits are typically 0.1–8 ppm for trace elements, 0.01–0.1 wt% for major elements and 0.1–0.01 ppm for REEs. The geochemical standards STD SO-18, STD DS7 and STD CSC were used to assess the accuracy of the analytical data. The quality of the analyses was determined using a range of reference materials (http://acmelab.com/services/method-descriptions/soiltill-and-sediment/).

4 Host Rock (Alkali Basalt-Dolerite)

Alkali basalt (doleritic basalt), called as Kocakızıl dolerite [88, 89], is observed as a horizon on the neritic dolomites in an extension of 15–20 km from Şarkikaraağaç to Yalvaç district in the western part of the Sultandağ Mountains and reaches a thickness of 30–40 m in the NW–SE direction. The doleritic basalt starts as a red altered flow above the dolomites

Table 1 Chemical analyses of the Sücüllü (Yalvaç, Isparta) lateritic bauxite deposits

	Bedrock	Weathered rock	Clayey lateritic bauxite			Ferrigenous lateritic bauxite								Bauxite
	BHVO-2	SL-1	SL-2	SL-3	SL-4	SL-5	SL-6	SL-7	SL-8	SL-9	SL-10	SL-11	SL-12	SL-13
SiO_2	49.60	40.56	35.34	35.10	37.13	20.84	30.31	32.40	26.28	31.50	17.95	34.95	22.50	7.52
Al_2O_3	13.44	15.92	20.43	20.70	22.19	20.61	25.08	26.17	20.01	28.16	23.20	32.22	33.80	49.99
Fe_2O_3	12.39	11.43	12.13	12.84	17.40	37.25	23.25	20.66	25.06	19.90	37.31	7.68	17.11	14.94
MgO	7.26	7.57	7.26	7.36	1.22	0.64	0.37	0.42	0.82	0.18	0.48	0.41	0.17	0.31
CaO	11.40	2.92	1.76	2.22	1.63	0.85	2.16	1.74	5.13	0.81	1.13	0.84	3.05	1.40
Na_2O	2.22	1.04	0.06	0.05	0.10	0.04	0.09	0.08	0.03	0.05	0.02	0.03	0.02	0.01
K_2O	0.51	2.71	1.86	2.09	3.05	0.55	0.61	0.56	1.19	0.17	0.62	0.68	0.27	0.03
TiO_2	2.73	2.05	2.57	2.63	2.84	2.52	3.04	3.10	3.04	4.36	4.33	5.25	6.75	10.70
P_2O_5	0.27	0.33	0.67	0.80	0.51	0.20	0.76	0.54	0.16	0.42	0.21	0.15	0.12	0.13
MnO	0.17	0.19	0.13	0.10	0.05	0.05	0.11	0.09	0.02	0.04	0.04	0.02	0.01	0.08
Sc	31.83	23.00	29.00	30.00	33.00	43.00	43.00	44.00	25.00	43.00	38.00	42.00	46.00	66.00
Ni	119.80	91.90	117.60	141.90	225.30	58.50	166.90	160.30	31.80	69.60	43.80	33.20	13.30	39.00
Co	44.89	53.30	75.20	63.60	59.70	59.10	80.60	64.20	10.40	23.20	23.50	23.30	7.20	51.80
Cr	287.20	814.51	390.14	273.79	308.01	349.08	451.75	61.60	82.14	335.39	451.75	561.26	629.71	1238.88
Ba	130.90	284.00	139.00	105.00	107.00	93.00	230.00	94.00	63.00	79.00	147.00	75.00	61.00	160.00
Cs	0.10	0.40	0.60	1.10	0.60	0.90	0.20	0.20	1.00	0.10	1.70	0.90	0.70	0.10
Rb	9.26	18.90	21.70	27.00	33.10	11.40	4.40	4.20	20.30	1.60	21.10	14.30	6.50	1.20
Sr	394.10	99.80	31.50	103.00	48.70	111.60	200.80	98.60	65.40	23.04	85.00	92.10	187.30	97.10
Zr	171.20	131.60	168.30	174.80	183.00	194.10	205.70	200.00	241.10	283.70	222.60	317.40	413.40	533.50
Hf	4.47	3.40	4.10	4.10	4.50	5.10	5.10	5.00	6.20	7.10	5.70	8.10	10.80	13.20
Ga	21.37	19.30	36.00	42.60	29.10	29.90	41.30	35.20	23.70	38.20	33.10	41.00	47.30	81.90
Nb	18.10	22.90	28.70	30.00	30.90	27.30	28.40	27.50	35.60	51.50	40.70	52.00	72.40	92.40
Th	1.22	2.70	3.20	3.30	3.80	5.30	3.80	3.80	7.20	5.90	5.90	8.00	11.70	14.50
U	0.41	0.60	1.00	1.50	0.90	4.20	0.90	1.10	3.30	1.80	4.90	3.20	20.40	4.30
V	318.20	262.00	292.00	249.00	324.00	419.00	283.00	326.00	390.00	389.00	378.00	458.00	580.00	775.00
Y	25.91	16.70	33.30	39.30	47.70	49.50	52.80	27.80	20.50	14.40	46.60	24.10	23.10	19.60
Cu	129.30	35.00	158.00	44.20	15.60	13.10	17.40	18.60	22.80	67.80	14.40	34.40	18.80	586.90
Pb	1.65	0.90	1.20	1.40	3.70	5.00	2.70	3.20	5.90	3.30	7.30	3.60	10.50	1.60
Zn	103.90	116.00	136.00	89.00	92.00	196.00	72.00	76.00	53.00	56.00	110.00	68.00	10.00	60.00

Table 1 (continued)

	Bedrock	Weathered rock	Clayey lateritic bauxite			Ferrigenous lateritic bauxite								Bauxite
	BHVO-2	SL-1	SL-2	SL-3	SL-4	SL-5	SL-6	SL-7	SL-8	SL-9	SL-10	SL-11	SL-12	SL-13
Ta	1.15	1.40	1.70	1.80	1.80	1.70	1.80	1.80	1.90	3.00	2.40	3.00	4.50	5.20
La	15.20	16.70	24.20	29.70	33.60	27.90	56.40	24.40	26.20	98.60	24.60	33.60	47.20	27.40
Ce	37.53	35.30	51.80	60.10	54.90	65.70	94.50	54.80	38.50	80.60	50.30	61.90	84.20	36.40
Pr	5.34	4.14	6.38	7.82	7.13	8.04	18.36	7.53	5.43	17.79	6.96	8.41	9.71	4.92
Nd	24.27	17.40	27.10	31.80	26.70	37.90	80.40	33.00	20.90	58.40	32.00	34.90	35.20	18.10
Sm	6.02	3.81	6.13	7.67	5.21	9.24	15.80	7.58	4.40	8.93	8.28	8.78	5.99	3.20
Eu	2.04	1.27	2.32	3.18	1.54	3.14	5.23	2.62	1.28	2.75	2.76	3.04	1.72	0.95
Gd	6.21	3.95	7.03	8.75	4.84	11.09	15.29	7.28	3.89	7.11	10.00	9.81	4.92	3.10
Tb	0.94	0.63	1.10	1.38	0.78	1.68	2.18	1.16	0.61	0.90	1.53	1.54	0.78	0.50
Dy	5.28	3.39	6.14	7.70	4.60	9.16	11.09	6.01	3.34	4.15	8.21	8.69	4.54	3.10
Ho	0.99	0.67	1.16	1.41	0.91	1.72	1.90	1.12	0.65	0.62	1.60	1.63	0.91	0.63
Er	2.51	1.75	3.12	3.53	2.60	4.45	4.62	2.87	1.72	1.50	4.05	4.18	2.68	1.89
Tm	0.33	0.26	0.42	0.48	0.39	0.59	0.59	0.41	0.25	0.21	0.54	0.57	0.40	0.29
Yb	1.99	1.54	2.40	2.59	2.30	3.26	3.43	2.51	1.51	1.36	3.07	3.27	2.58	1.81
Lu	0.28	0.21	0.33	0.36	0.35	0.48	0.46	0.35	0.23	0.19	0.43	0.43	0.38	0.28
∑REE	108.94	91.02	139.63	166.47	145.85	184.35	310.25	151.64	108.91	283.11	154.33	180.75	201.21	102.57
Ti/Al	0.20	0.13	0.13	0.13	0.13	0.12	0.12	0.12	0.15	0.15	0.19	0.16	0.20	0.21
Sm/Nd	0.25	0.22	0.23	0.24	0.20	0.24	0.20	0.23	0.21	0.15	0.26	0.25	0.17	0.18
Th/Sc	0.04	0.12	0.11	0.11	0.12	0.12	0.09	0.09	0.29	0.14	0.16	0.19	0.25	0.22
La/Cr	0.05	0.02	0.06	0.11	0.11	0.08	0.12	0.40	0.32	0.29	0.05	0.06	0.07	0.02
La/Y	0.59	1.00	0.73	0.76	0.70	0.56	1.07	0.88	1.28	6.85	0.53	1.39	2.04	1.40
(La/Yb)cn	5.15	7.33	6.81	7.75	9.87	5.78	11.11	6.57	11.72	48.99	5.41	6.94	12.36	10.23
Eu/Eu*	1.18	1.17	1.13	1.13	1.23	1.10	1.21	1.21	1.25	1.30	1.10	1.14	1.29	1.21
Ce/Ce*	0.97	0.91	0.91	0.86	0.73	0.98	0.67	0.91	0.66	0.38	0.85	0.79	0.80	0.62
CIA	35.62	63.47	84.64	82.26	80.99	92.27	89.58	90.94	66.06	97.46	91.14	94.28	85.82	95.63
IOL	34.24	40.27	47.95	48.86	51.60	73.52	61.46	59.11	63.17	60.41	77.12	53.31	69.35	89.62
MIA (R)	21.00	30.89	40.66	39.82	53.35	43.17	57.29	60.82	41.37	66.96	45.95	80.32	66.62	79.86

BHVO-2: Basalt, Reference standard material (USGS)

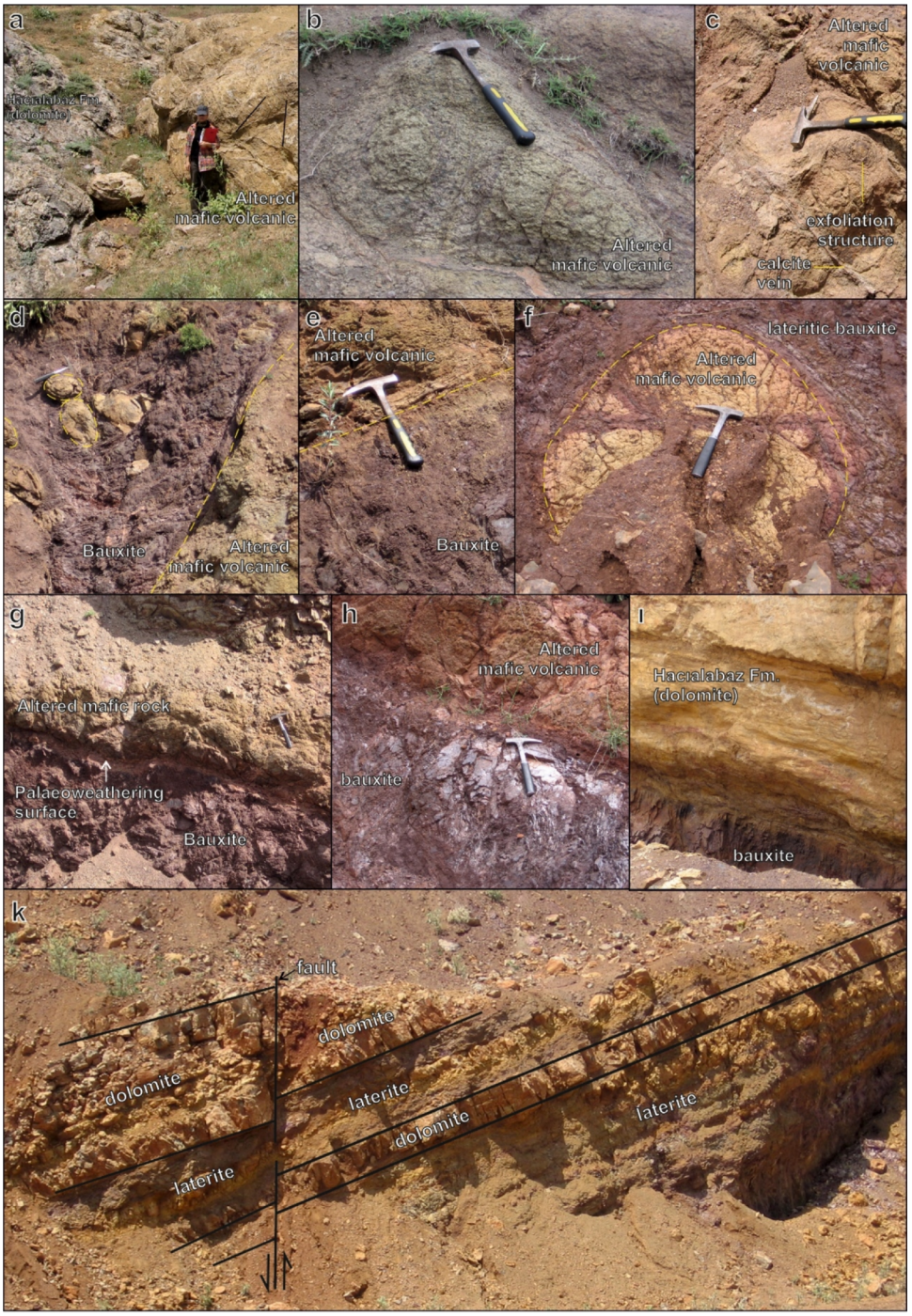

Fig. 3 **a** Stratigraphic contact between Hacıalabaz limestone and mafic volcanic, **b** Altered mafic volcanic, **c** altered mafic volcanic cutting calcite veins and showing exfoliation structure, **d**, **e** contact of bauxite and mafic volcanic, **f** contact of lateritic bauxite and altered mafic volcanic, **g** contact showing paleoweathering surface and altered mafic rock, **h** contact between altered mafic volcanic and bauxite, **ı** sharp contact of Hacıalabaz limestone and bauxite, **k** alternating between laterite and dolomite suggesting transportation

(Fig. 3A). It changes towards the top to fresh pillow basalts (Fig. 3B) and also occurs in pale green, greenish and black colours and is also cut by abundant secondary calcite and silica veins (Fig. 3C). It commonly displays a spectacular exfoliation structure in region (Fig. 3C). Eren [88] stated that the age of the doleritic basalts was considered as a possible Triassic age. However, the Jurassic age of the dolomitic carbonates belonging to the Hacıalabaz Formation corresponds to the same age of the doleritic basalt. In the north-western part of the Sultandağ Mountains (Sağır district, 15 km northwest of the Sücüllü area), both basement units and dolomitic carbonates are cut as dyke by these doleritic basalts ([89, 90], p 22). This stratigraphic significance suggests that the doleritic basalts may be of Jurassic age. Öncel [54] suggests that the age of the doleritic basalt is Upper Kimmeridgian (Upper Jurassic) considering the age of the carbonate rocks in the region.

5 Topographic Features and Lateritic Bauxite Horizon

The geomorphology of the study area is characterised by rugged topography with the peak (Karaçalı Hill, 1853 m) at the NW–SE trending Sultandağ Range, separated by SW-NE trending valleys. The topography varies from rolling hills and moderate relief at elevations up to 1100 m, to high plateaus and sharp-topped ridges at elevations above 1500 m above mean sea level. The lateritic horizons are well exposed at Uzunalan Hill (1649 m) and Kuşyakası area (~ 1350 m) along the NW foothills of the Sultandağ Range (Fig. 2B). It is noted that the terrain, a slope of less than 45°, has a well-developed lateritic bauxite horizon (38°20′44.79"K, 31°11′10.16"D, 1298 m) above the doleritic basalt rocks, located in the eastern part of Sücüllü village (Yalvaç, Isparta). This horizon is found on the doleritic alkaline basalt and ranges from 1 to 30 m in thickness (Fig. 3D). The contact relationship between altered pillow lava-shaped mafic volcanic and bauxite is mostly sharp, and in some locations a paleoweathering surface is observed between altered mafic volcanic rock on bauxite (Fig. 3D–H). The upper stratigraphic contact coincides with the hanging-wall limestone (Fig. 3I). The contact between the lateritic bauxite horizon and the underlying doleritic basalt bedrock is transitional. The top of the lateritic horizon is cut by later weathering iron oxide phases (e.g. hematite, goethite). In the upper part of the lateritic horizon, transported lateritic soils without host doleritic basalt are observed alternating with thin-bedded neritic dolomites (Fig. 3K) and also they are cut by faults of the Miocene tectonic regime. This suggests that while the deposition of dolomites continues in the shallow environment, the rapid transport of lateritic formations formed on land during bauxitisation processes to the marine environment is indicated by the sudden uplift of the region with normal block faulting. In support of this view, Ayhan and Karadağ [25] stated that the bauxitic horizon in certain locations in the south-eastern part of the Fele region contains well-rounded pebbles of doleritic basalt and bauxite, indicating transport. The variation in thickness is caused by topographic morphology displacement and bedrock position in region. Bauxite deposits, which were operated in previous years, are currently not actively operated due to the change in thickness. In region, most deposits are now sub-economic and can be operated economically in the future.

6 Results

6.1 Mineralogical Composition

Based on mineralogical and petrographical studies of thin sections, the Sultandede Formation consists mainly of phyllite and metasandstone lithologies. Its mineral paragenesis of the phyllite is quartz, plagioclase, sericite and chlorite. Metasandstone is mainly composed of quartz, calcite, muscovite, plagioclase, sericite and opaque minerals [26]. The dolomitic limestone of Hacıalabaz consists mainly of micritic and sparry calcite in the breccias, euhedral dolomite in the biomicritic limestone and some Jurassic fossils such as *Orbitolina* sp. and *Cuneolina* sp. (Fig. 4A–D). Weathered mafic basalts consist mainly of plagioclase, augite, calcite and opaque minerals (hematite, magnetite) and show a coarse doleritic crystalline texture (Fig. 4E). Augite usually occurs as euhedral, subhedral prismatic crystals. Clay minerals can be clearly defined along the albite twin lamellae in plagioclase with secondary silica between long rod crystals. Occurrences of palagonite, an alteration product resulting from interaction between water and basaltic lava, are common in weathered doleritic basalt (Fig. 4F).

The mineral paragenesis of the lateritic bauxites in the Sücüllü region consisted of gibbsite, boehmite, hematite, kaolinite, smectite, feldspar, chlorite, ilmenite, anatase as identified by XRD (Fig. 5A–D) and SEM determinations (Fig. 5E–K). Fragments of volcanic glass in an amorphous matrix show possible palagonitisation and rhombohedral calcite crystals of carbonate phases in weathered mafic volcanic rock (Fig. 5F). Euhedral calcite crystals typically occur in samples with high carbonate phases (Fig. 5F). The principal clay minerals are kaolinite and smectite. In the clayey laterite zone, kaolinite clusters can be observed along the pores (Fig. 5H). Fe-rich haematite phases are formed (Fig. 5I). Gibbsite and boehmite are observed together with kaolinite in the form of hexagonal plates (Fig. 5K). Kaolinite is a mineral formed as subhedral pseudo-hexagonal plates in an amorphous matrix. Its crystal size is generally less than 1 μm in samples.

Based on the mineralogical determinations, mineralogical and lithological properties along a 30 m profile, weathered mafic basaltic rock comprises feldspar, pyroxene and calcite minerals. Further up the profile, as it moves away from the bedrock, the feldspar minerals begin to change to clay (smectite) minerals. As the degree of weathering increases towards the middle of the profile, kaolinite minerals begin to form in addition to smectite minerals. Towards the upper parts of the profile, Fe-rich haematite and goethite are formed, and towards the top of the profile, kaolinite, boehmite and gibbsite are formed (Fig. 6).

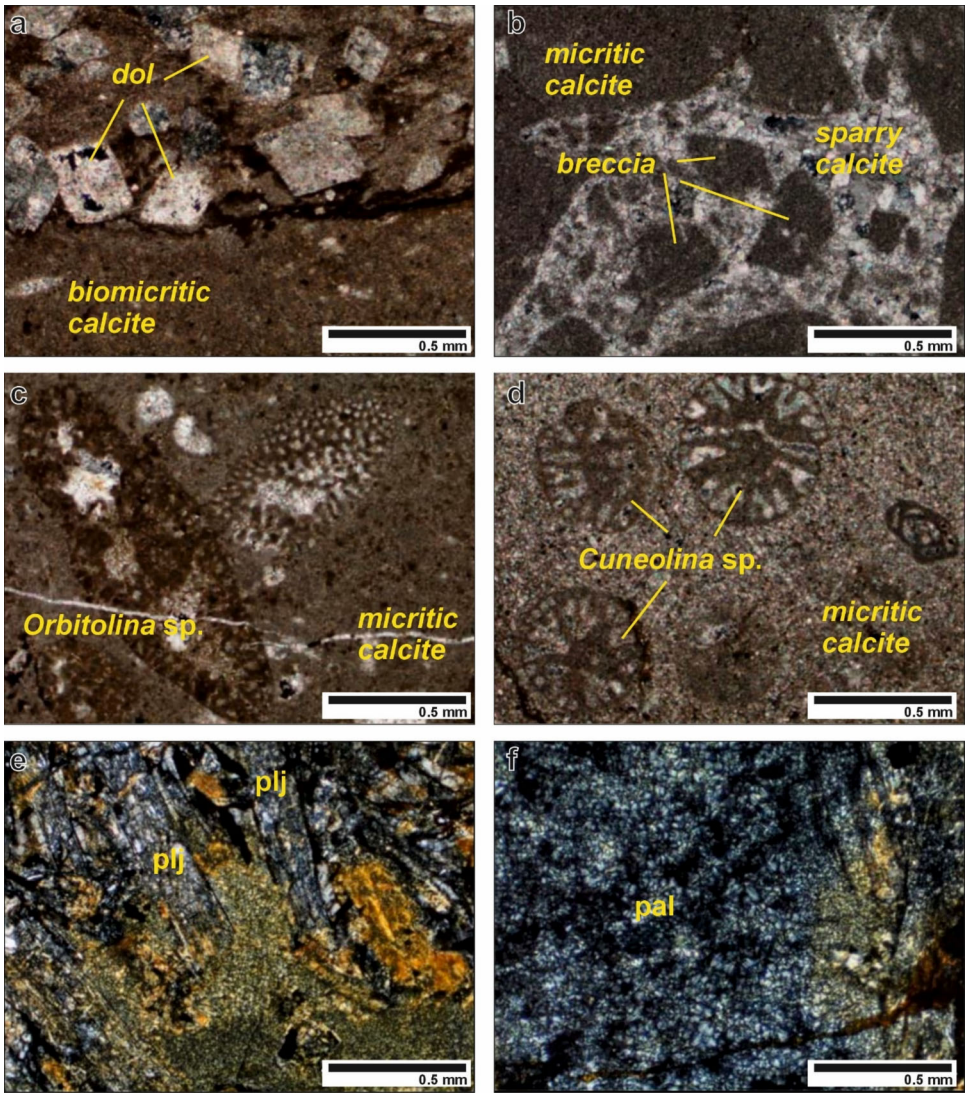

Fig. 4 **a**, **b** biomicritic calcite, micritic calcite and sparry calcite, breccia and dolomite crystals, **c**, **d** *Orbitolina* sp. and *Cuneolina* sp. fossils indicating Jurassic age in micritic calcite belonging to the Hacıalabaz limestone, **e**, **f** plagioclase crystals and palagonitasiton in altered mafic volcanic. dol: dolomite, plj: plagioclase, pal: palagonite

6.2 Geochemistry

The bulk rock compositions of thirteen samples of lateritic bauxites are presented in Table 1. The concentrations of Al_2O_3 (15.92–49.99 wt%), SiO_2 (7.52–40.56 wt%), Fe_2O_3 (7.68–37.31 wt%) and TiO_2 (2.05–10.7 wt%) are the highest among the major oxides in the analysed lateritic bauxite samples. The concentrations of total alkaline earth elements (Na + K) are low and fall in a narrow range (0.04–3.75 wt%).

The Sücüllü lateritic bauxites deposits are derived from alkali basaltic rocks. The most commonly used approach is the Zr/TiO_2 vs. Nb/Y diagram [91, 92], where Nb/Y indicates alkalinity ($Na_2O + K_2O$) and Zr/TiO_2 indicates silica. The Nb/Y ratio increases from sub-alkaline to alkaline compositions, while the Zr/TiO_2 ratio decreases from acidic to basic compositions. This diagram suggests that all lateritic bauxite samples fall into the basalt, alkaline basalt and rarely foidite character (Fig. 7A). They are of sub-alkaline to alkaline character. The major components of the Sücüllü lateritic bauxites were plotted in the ternary Al_2O_3–SiO_2–Fe_2O_3 diagram [8] (Fig. 7B). In this diagram, the studied samples plot in the fields of clayey bauxite, bauxitic clay bauxite, bauxitic clayey Fe ore and bauxite Fe ore. Based on the classification scheme of [93], the majority of the lateritic bauxite samples fall within the laterite and kaolinite field to lesser extent bauxite and bauxitic kaolinite, whereas one sample plots within the bauxite field (Fig. 7C). Compared to the reference basaltic rock (BHVO-2), Sücüllü lateritic bauxites have higher concentrations of Cr (mean 354.05), Zr (mean 236.74), Nb (mean 38.64) and Ga (mean 36.13).

A strong positive correlation between Al, Zr, Hf, Nb, Ta, Th and Ti indicates, in situ, the transformation of a Ti-rich parent rock (alkali basalt) into lateritic and bauxitic material during the weathering process (Fig. 8A–F). Trace elements like Nb and Ta correlate positively with TiO_2 ($r^2 = 0.96$ and

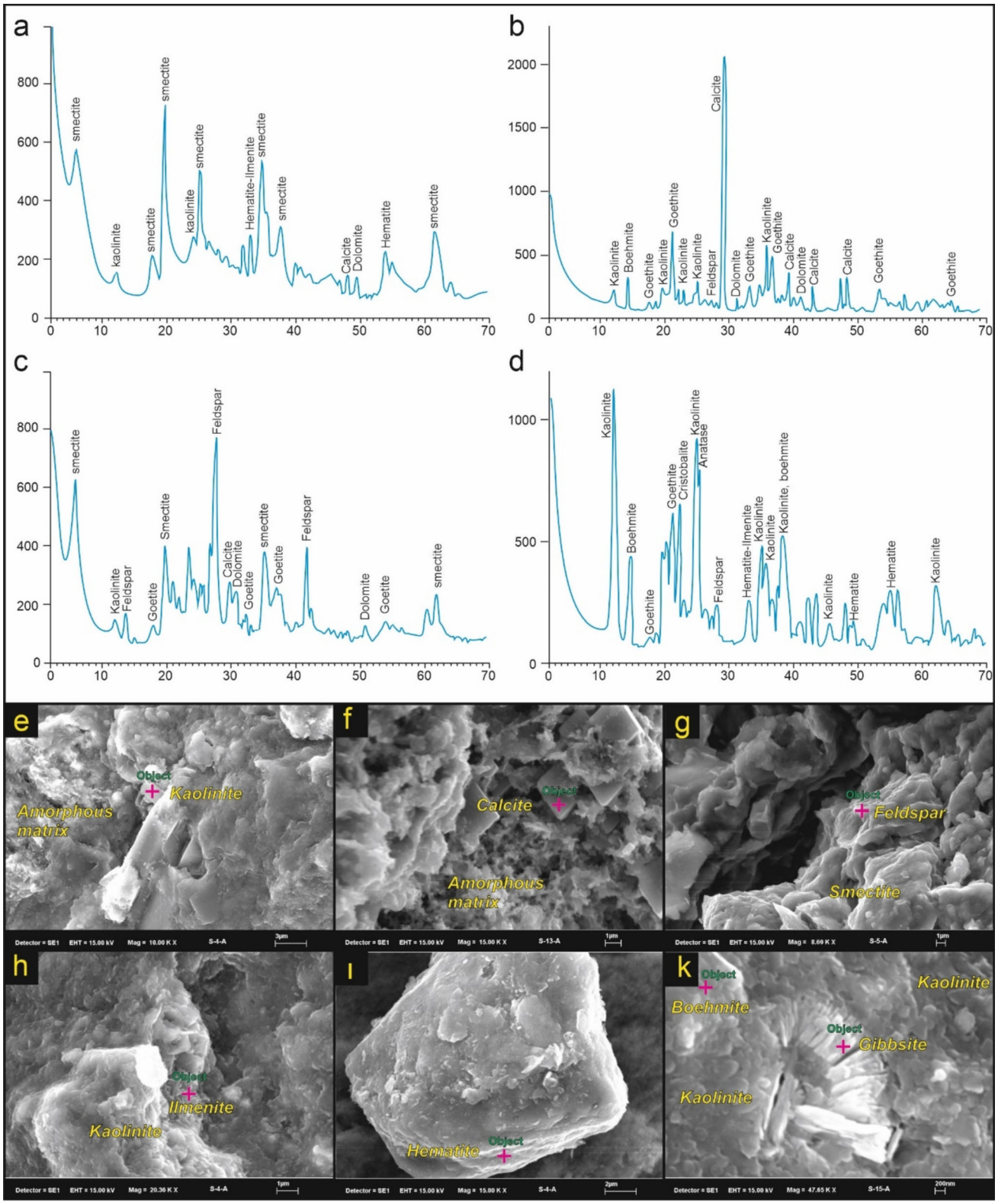

Fig. 5 **a**, **d** X-ray diffraction (XRD) patterns, **e**, **k** Scanning electron microscope (SEM) image of Sücüllü lateritic bauxite deposits

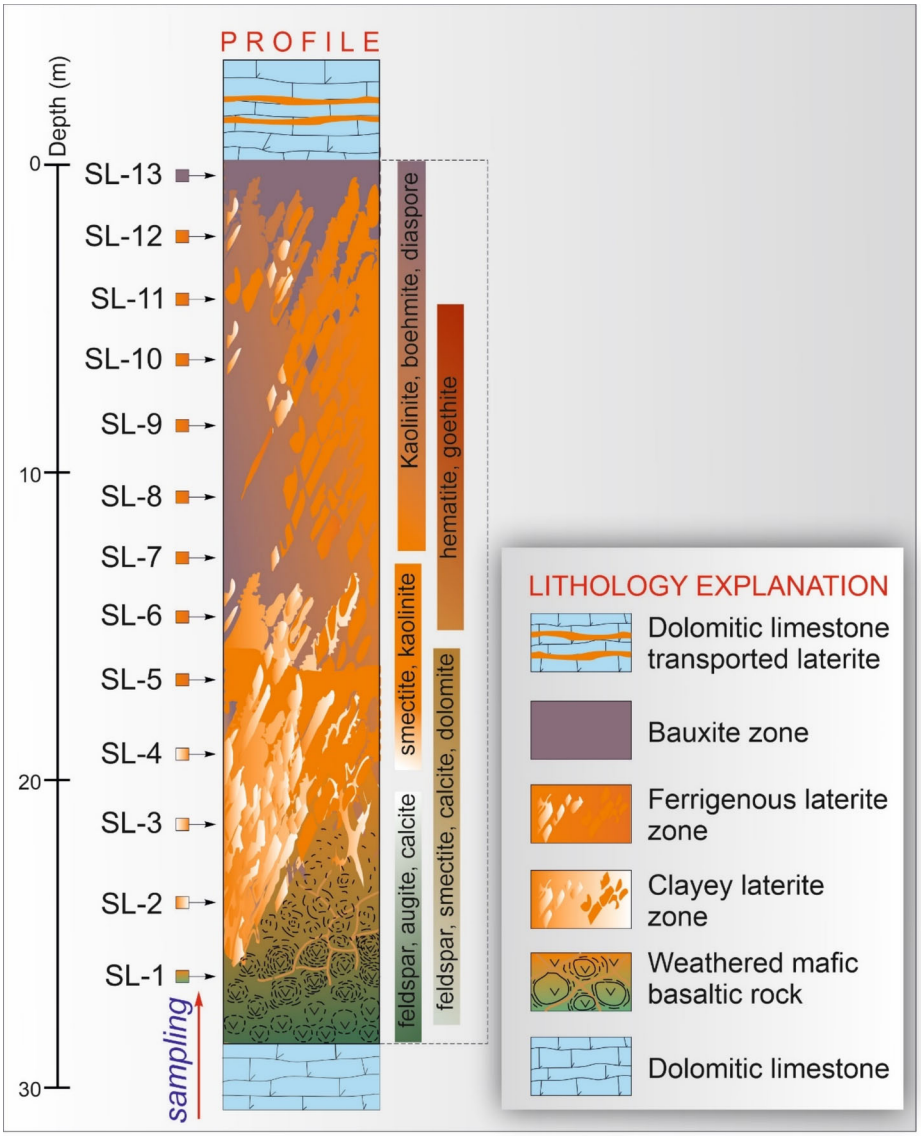

Fig. 6 Geological sketch section showing lithological description and mineralogical phases in weathering profile of the Sücüllü lateritic bauxite deposits

0.94, respectively); however, Nb and Ta have a strong positive inter-element correlation ($r^2 = 0.96$). The enrichment of Nb and Ta in bauxite and lateritic bauxite samples is suggested by their strong positive correlation with Ti-bearing anatase or ilmenite. The association between Nb and Ta with anatase and ilmenite was also confirmed by XRD pattern (see Fig. 5A–D). Ga is enriched with aluminium during lateritisation. The relationship between Sc and Ti indicates the presence of mafic (pyroxene) mineral in the Ti-rich bedrock. The association and relationship of Nb, Ta and V indicates rutile or ilmenite phases in the basaltic parent rock. Cr, a strong immobile element, emphasises the presence of a ultramafic mineral (olivine) in the precursor rock. Hf and Zr indicates association with heavy mineral (zircon).

Compared to the parent rock (Hawaiian basalt, BHVO-2), the chondrite-normalised REE pattern of lateritic bauxite samples reflects a slight enrichment in REE, and they suggest a pattern similar to Payas and Çarıksaraylar bauxite deposits, southern Turkey (Fig. 9). Basic rocks show weak or no Eu/Eu* anomaly, whereas felsic rocks generally have well-developed negative trend. Eu anomaly pattern is reflected in the dissolution of plagioclase or other Eu enriched minerals during chemical weathering [94]. In chondrite-normalised diagram, Sücüllü samples show weak or no Eu/Eu* anomaly ranging from 0.92 to 1.19 with average 1.01, suggesting the basic origin. Compared with data of bauxite deposits in world, Sücüllü samples show no Eu anomaly similar to the bauxite deposits derived from basic precursor such as Payas (Türkiye), Çarıksaraylar (Türkiye) and Kabirdham (India); however, other bauxite deposits, especially karstic bauxites, originated from dominantly intermediate source rocks

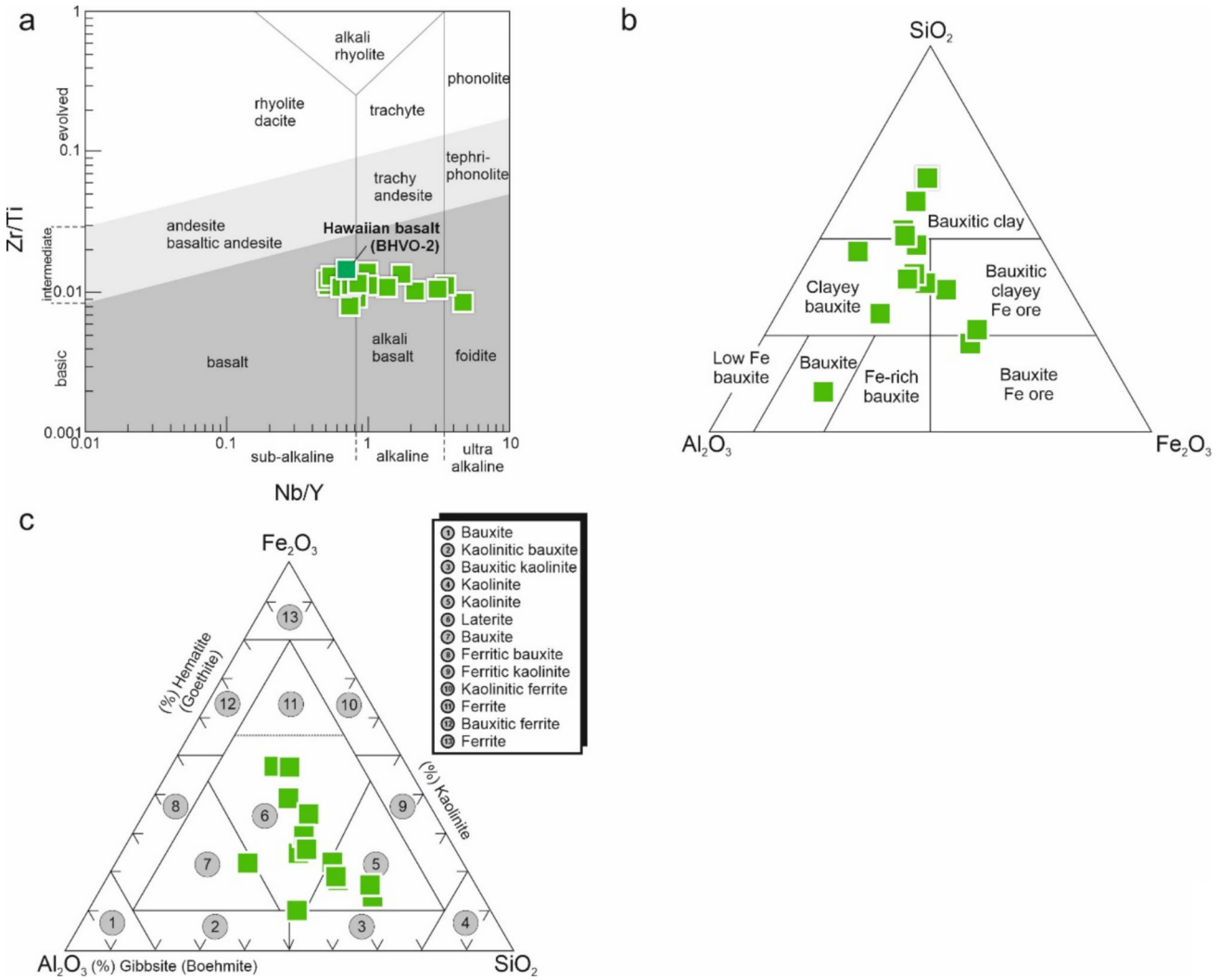

Fig. 7 **a** Zr/TiO_2 vs. Nb/Y diagram for the Sücüllü lateritic bauxite samples [92], suggesting alkali basalt nature for the parent rock, **b** Ternary plot for the system of Fe, (Al + Ti) and clay minerals [8] showing the position of the studied lateritic bauxite samples, **c** Plot of studied samples in a Fe_2O_3-Al_2O_3-SiO_2 ternary diagram after [93]

and exhibited moderately to strongly negative Eu anomaly (Fig. 9).

Al/Ti ratio is used in identification of source rocks in clastic sedimentary rocks [95]. This ratio seems to be applicable also in the origin studies of bauxite deposits. This ratio typically ranges from 3 to 8 in mafic, 8–21 in intermediate and 21–70 in felsic igneous rocks [96]. Al/Ti ratio of the Sücüllü lateritic bauxite deposits varying between 4.67 and 8.44 (average 6.96) falls between the ratio given for mafic rocks, but is slightly higher than that of Hawaiian alkali basalt (4.92). It is emphasised that the Manisa (Menderes massif, western Turkey) metamorphosed karst bauxites of Upper Cretaceous are high critical metals (mean ∑REY 5195 ppm, Li 284 ppm, B 164 ppm). They have negative Eu anomaly with high Al/Ti (23.30), suggesting felsic igneous source (unpublished data). Similarly, Upper Carboniferous karst bauxites of North China Craton have highly Li (892 ppm) and B (327 ppm) and moderately ∑REY compositions (675 ppm) [97], with negative Eu anomaly values, and high Al/Ti ratio (39.84) indicates that felsic precursor.

7 Discussion

7.1 Paleoweathering and Lateritisation/Bauxitisation Processes

The degree of weathering can be measured by means of various chemical indices [98]. The Chemical Index of Alteration (CIA: [99, 100]) is a tool for quantifying chemical changes

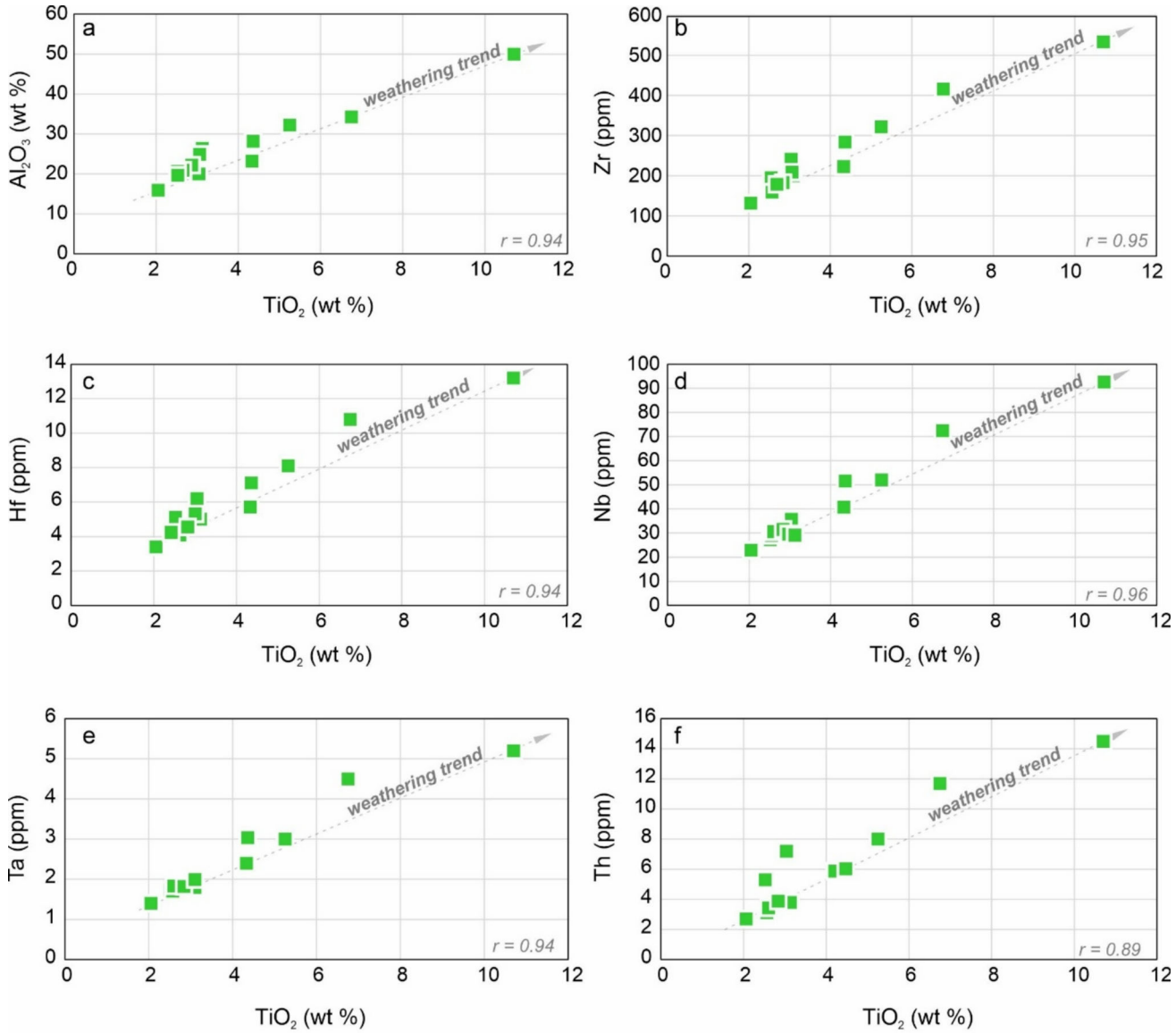

Fig. 8 **a–f** Correlation diagrams illustrating weathering trend and positive relationship between Al_2O_3, Zr, Hf, Nb, Ta, Th and TiO_2

during weathering processes. The CIA is calculated as CIA $= [(Al_2O_3)/(CaO^* + Na_2O + K_2O + Al_2O_3)] \times 100$, where the oxides are expressed as molar proportions and CaO* is CaO only in silicates (as opposed to that in phosphates or carbonates). On the other hand, if $CaO < Na_2O$, molecular CaO is accepted as a proxy for CaO*. Highly weathered laterites are indicated by the high ratios [101], and also, their CIA values range from 63.47 to 97.46 (average = 85.73), indicating strong intensity of chemical weathering (Fig. 9A). [99] highlighted that high ratios of CIA are an indication of aggressive weathering under hot humid, warm conditions, possibly in a tropical conditions. Therefore, intense chemical weathering under warm and humid conditions is suggested by the high CIA values (> 85) and kaolinite, gibbsite-dominated mineral composition of the Sücüllü lateritic bauxite deposits (Fig. 10A, [100, 102]).

More recently, Babechuk et al. [103] proposed the "mafic index of alteration" (MIA), which is similar to the CIA but incorporates the behaviour of the mafic elements Fe and Mg in addition to Ca, Na and K with respect to Al to quantify the degree of lateritisation. Furthermore, to quantify the redox-dependent weathering behaviour of Fe/Al in lateritic/bauxitic profiles, Babechuk et al. [103] factored MIA into $MIA_{(o)}$ and $MIA_{(R)}$, which are applicable to the enrichment of Fe and Al, respectively, in weathering profiles. The Al_2O_3–$CaO + Na_2O + K_2O$–Fe_2O_3–MgO ternary diagram shows that Sücüllü lateritic bauxites have from 30 to 80 MIA values and trend ranging from the Fe–Mg apex to the Al apex, enriched in smectite and kaolinite (Fig. 10B).

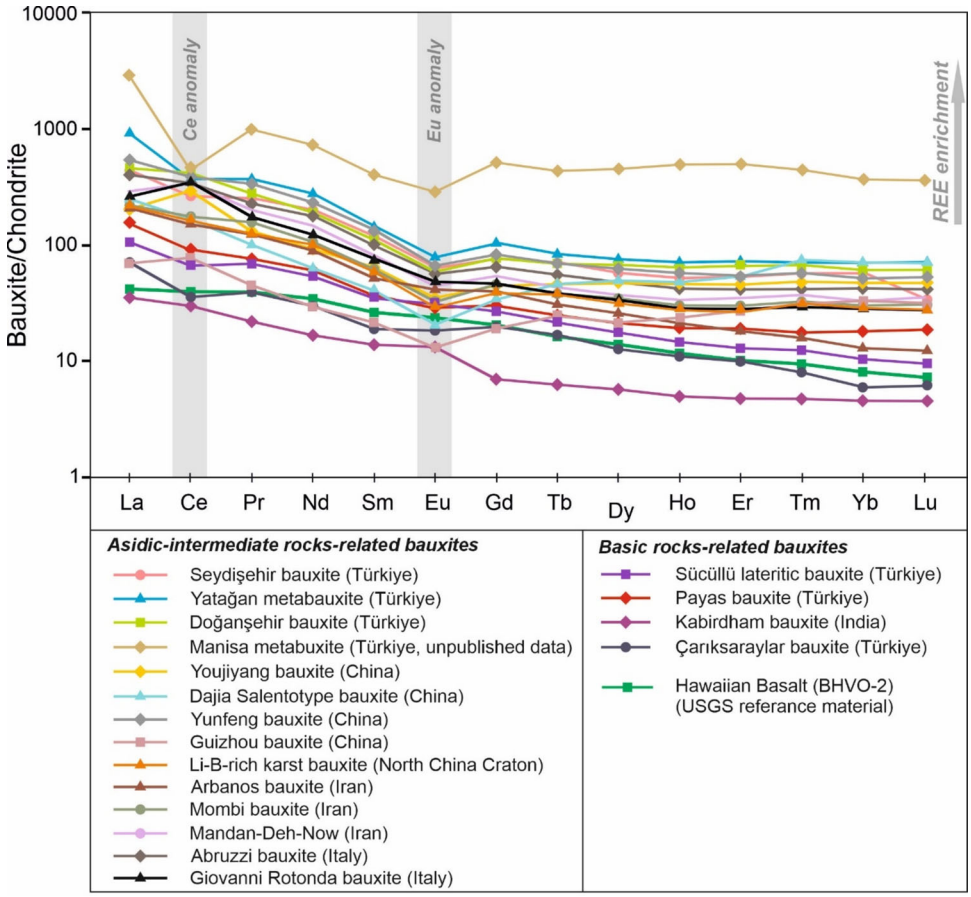

Fig. 9 Chondrite-normalised diagram depicting the rare earth element (REE) patterns of the Sücüllü lateritic bauxites and different bauxite deposits from world

Schellmann [104, 105] suggested the Si-Al–Fe triangular diagram to quantify the degree of lateritisation and to distinguish between kaolinitised, weakly, moderately, strongly lateritised and bauxitised. In this diagram, the Sücüllü lateritic bauxites mostly comprise a trend with gradual change from SiO_2-rich to $Fe_2O_{3\_}$ and Al_2O_3-rich compositions (Fig. 10C), and they are commonly kaolinitised, weakly lateritised and rarely moderate-to-strong lateritised (Fig. 10C). [103] also introduced the use of the $SiO_2/(Al_2O_3 + Fe_2O_3)$ ratio as an index of lateritisation "IOL", which can be obtained using the weight % ratio of SiO_2, $Fe_2O_{3(T)}$ and Al_2O_3 according to the following equation:

$$IOL = 100 \times [(Al_2O_3 + Fe_2O_{3tot})/(SiO_2 + Al_2O_3 + Fe_2O_{3tot})]$$

Due to their high Ti, Nb, V, Sc element contents, lateritic bauxites in Sücüllü region were derived from Ti-rich basaltic rocks, similar to the Hawaiian basalts from the Halemaumau Crater in Kilauea Caldera of Hawaii (USA). Of these basalts, the BHVO-2 sample is used in this study for comparison with the USGS Mafic Reference Rock. Unweathered mafic rocks have IOL values that are generally less than 40, as indicated by the basalt rock (BHVO-2). Fe and Al are particularly concentrated towards the upper part of the profile. Si is depleted in the upper part of the lateritic horizon. Ni, Co, Y, which behave as "mobile elements" in bauxitic soils, show the lowest concentration in the upper parts. Zr, Ga, Ta, Cr, which are immobile, are mostly concentrated in the upper part of the weathering profile, similar to the pattern in bauxitic rocks. The IOL values of the Sücüllü lateritic bauxites vary between 25.22 and 82.35 from weak lateritisation to strong lateritisation (Fig. 10C). The MFW ternary diagram [106] is another advanced scheme based on the combination of major elements to identify the effects of chemical weathering. In ternary diagram, M and F vertices indicate mafic and felsic source rocks, respectively. The W vertex shows the degree of weathering of the sources. The bulk density decreases as the intensity of weathering increases within the profile. In the relationship between Mafic (M)-Felsic (F)-Weathering (W), the studied lateritic bauxite samples show trend closer to basaltic weathering line between M and W apex suggesting intense weathering with a bulk density of 1.55 (Fig. 10D). According to the M-F-W ternary diagram, all of the studied lateritic samples cluster in the W corner, except one sample (Fig. 10D). This suggests that the Sücüllü lateritic bauxite samples are strongly weathered under the acidic conditions. Acidic or alkaline conditions with changes

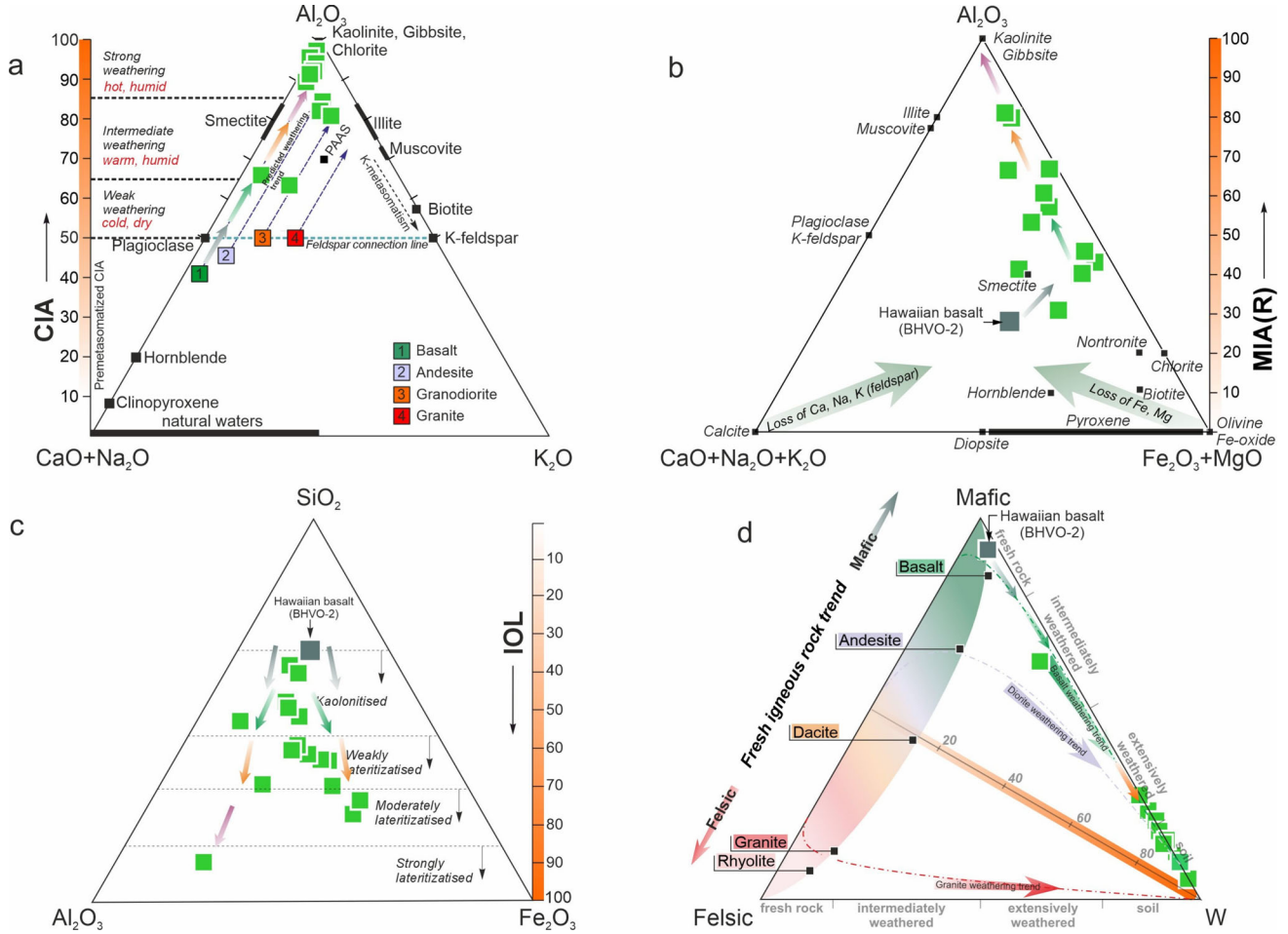

Fig. 10 **a** Chemical index of alteration ternary plot of molecular proportions Al_2O_3-(CaO* + Na_2O)-K_2O showing the weathering trend in the Sücüllü lateritic bauxites after [100], **b** Al_2O_3-CaO* + Na_2O + K_2O-$Fe_2O_{3(tot)}$ + MgO plot [99, 100], **c** SiO_2–Al_2O_3–$Fe_2O_{3(tot)}$ ternary plots illustrating mafic index of alteration along weathering profile [103], **d** mafic-felsic-weathering (W) ternary plot of [106]

in pH during bauxitisation are also confirmed by La/Y variations [107, 108]. Thus, La/Yb < 1 values are indicative of acidic conditions, while values of La/Y > 1 are indicative of alkaline conditions. The La/Y ratios in samples from Sücüllü lateritic bauxite deposits range from 0.56 to 6.85 (average 1.48). The La/Y values indicate that the samples closer to the bedrock are basic, while the samples closer to the upper part of the profile reflect acidic conditions during bauxitisation. Similarly, $(La/Yb)_{cn}$ values also support this result.

Mineralogical analysis of the lateritic bauxite ore indicates that the major mineral constituents are boehmite, kaolinite, smectite, illite and hematite, with boehmite, gibbsite, kaolinite, smectite, feldspar, hematite, goethite and anatase as minor minerals. Other minerals such as ilmenite, quartz, dolomite and calcite are also present as minor constituents. In the terrestrial environment, the basalts have been subjected to acid leaching with percolation along their fractures and cracks of acidic solutions since the pH decreased below 4. Low values of immobile elements (e.g. Sc, Th, Nb, Zr) indicate that the clayey laterite zone first appeared with the weathering of the basaltic bedrock. In this zone, the leaching process caused the formation of clay minerals (smectite) from feldspar-rich minerals. During the weathering of lateritic bauxites, Al-rich mixtures were initially deposited as boehmite and later led to the formation of boehmite to gibbsite. Intensive acid leaching of the basaltic bedrock to smectite and the ferromagnesian minerals (olivine, augite, pyroxene) occurred in the ferruginous laterite zone to iron. As weathering continued, bauxite became the most common product. When the environment was subsided with faults, thin-bedded dolomites started to be deposited on laterites and bauxites in the sea. Immediately afterwards, with the terrestrialisation of the environment, laterites and bauxites in the terrestrial environment began to be transported and re-deposited on dolomites in the marine environment.

7.2 Genetic Implications and Parental Affinity

As introduced earlier, a genetic classification of bauxite deposits into three groups such as (i) lateritic, (ii) tikhvin and (iii) karstic bauxites is based on their occurrence and formation [8]. Of these, lateritic-type bauxite deposits are directly related to the weathering of the underlying aluminosilicate rocks by their preserved textures and compositions and are also the main source of bauxite worldwide (about 88%) [8, 38, 109, 110]. Tikhvin-type bauxites are detrital bauxite deposits overlying the eroded surface of aluminosilicate rocks and are also the eroded products of lateritic bauxite deposits. Karstic-type bauxite deposits are formed by the deposition of Al-rich laterite on karst depressions and sinkholes of carbonate lithologies (limestone, dolomite and rarely marl) [3]. Other classifications of bauxite deposits include their mineralogical composition, geomorphology and hydrogeological position [111, 112]. Das et al. [113] stated that the Darai-Daldali lateritic bauxite deposits are developed from weathering of basaltic rocks. Their mineralogical compositions composed of gibbsite and boehmite and anatase and brookite as accessory minerals.

Lateritic products (Al-rich bauxites or Fe–Ni-Co-rich laterites) are widely recognised as regional markers for a variety of large-scale events [114]. For this reason, bauxite deposits of different types in general, such as karstic, Fe-Ti bauxite and laterite, and especially those originating from the interior of thick carbonate basins, such as the Tauride orogeny in the Eastern Mediterranean, have typical geochemical characteristics which are useful in solving certain problem relating to their source rocks. Bedrock composition is also significant, with aluminium-rich rocks (Al 10%) favouring bauxite formation [109, 115]. Earlier efforts have attempted to solve parent rock of bauxites using various immobile elements such as Ga, Cr, Ni, Th, Zr, Hf, Nb and Ta [8, 24, 25, 27–29, 36, 49, 52, 116, 117]. The source rock of the karst-type bauxite deposits currently being mined in the Seydişehir region (southern Turkey) is the Lower and the Upper Triassic pelitic rocks and shales and therefore has a more intermediate composition [see 29 for details]. In addition to these deposits, the origin of the metamorphosed karstic bauxite deposits (e.g. diasporite, corundite) exposed in the southern Menderes Metamorphic Massif (SW Turkey), which are commonly hosted in thick-bedded platform-type marbles, are similar to the karstic Taurian bauxites in the Central Taurides (Seydişehir region) and presumably of similar age (Cenomanian–Turonian) [49]. On the other hand, the Payas-Islahiye bauxite deposits, which are located in the same orogenic zone as the Seydişehir karst bauxite deposits, are basaltic in composition because their parent rocks are basaltic tuffs [35, 36]. Likewise, Sücüllü region (Yalvaç, Isparta) lateritic bauxite deposits, the main subject of this study, occur in two different types as in situ lateritic bauxite and transported lateritic bauxite.

The bauxite deposits exposed in the Tauride orogenic belt have different compositions, but were formed in the Late Cretaceous and have geochemical evidence that can help solve geological problems. The shallow marine platform carbonates of the Tethyan Ocean were deposited during the Triassic, Jurassic and Cretaceous along the Tauride orogenic belt [24–30, 45, 118], and also large-volume allochthonous bauxite deposits overlying a karstic palaeosurface in the Seydişehir region (Konya, SW Turkey), [24, 27, 29] are the karst-type deposits based on the classification of Bárdossy [8]. The provenance of karst bauxites in the Tauride belt has been investigated by many researchers using immobile elements such as Ga, Cr, Ni, Th, Zr, Hf, Nb and Ta [24, 29]. These researchers suggested that the nearby Ordovician metamorphic rocks, known as Seydişehir slates, were the source of the bauxite deposits in the region. In the Sücüllü region, the bauxite deposits are generally residual bauxite deposits formed by in situ and directly (autochthonous) lateritisation of sub-surface precursor rocks (altered alkali basaltic volcanics). As a result, the studied lateritic bauxites can be classified as laterite-type bauxites based on their geological and geochemical characteristics. This conclusion is further supported by [25, 36, 52]. According to the Ayhan and Karadağ [25], the formation of autochthonous iron bauxites in the Şarkikaraağaç region is entirely lateritic and derived from Jurassic-aged dolerites.

It is thought that Ti, Nb, Zr, Hf and Ta are immobilised during the ore-forming processes and are eventually enriched in the bauxite-bearing rocks [6, 9, 119, 120]. These elements are mainly enriched in the mineral Ti-dioxide and Zr and Hf are controlled by the mineral zircon in bauxites [110, 119, 121, 122]. On the Ga-Zr-Cr triangular diagram of Balasubramaniam et al. [123], Sücüllü lateritic bauxite samples cluster in the strongly basic range of the parental rock (Fig. 11A). In addition, rare earth elements were initially considered to be immobile or not to be fractionated during the weathering processes. In this context, the Eu/Eu* ratio shows a positive trend in the mafic rocks and a generally negative trend in the acidic rocks. All samples of the Sücüllü lateritic bauxites display traces of mafic precursor, as suggested by positive Eu anomalies (1.10–1.29). The Eu/Eu $*$ and the Sm/Nd ratios are considered to reflect the source rock of the bauxite, as only minor fractionation of Sm and Nd occurs during strong chemical weathering. The Eu/Eu $*$ vs the Sm/Nd diagram reflects that studied bauxite samples are derived from basalt (Fig. 11B). Titanium is immobilised during the processes that form the bauxitic ore. In the Eu/Eu $*$ vs. TiO_2/Al_2O_3 binary diagram, alkali doleritic basalt and its weathering products are close to basalt, but far away from granitic rocks (Fig. 11C). The Sm and Nd elements are more recently used

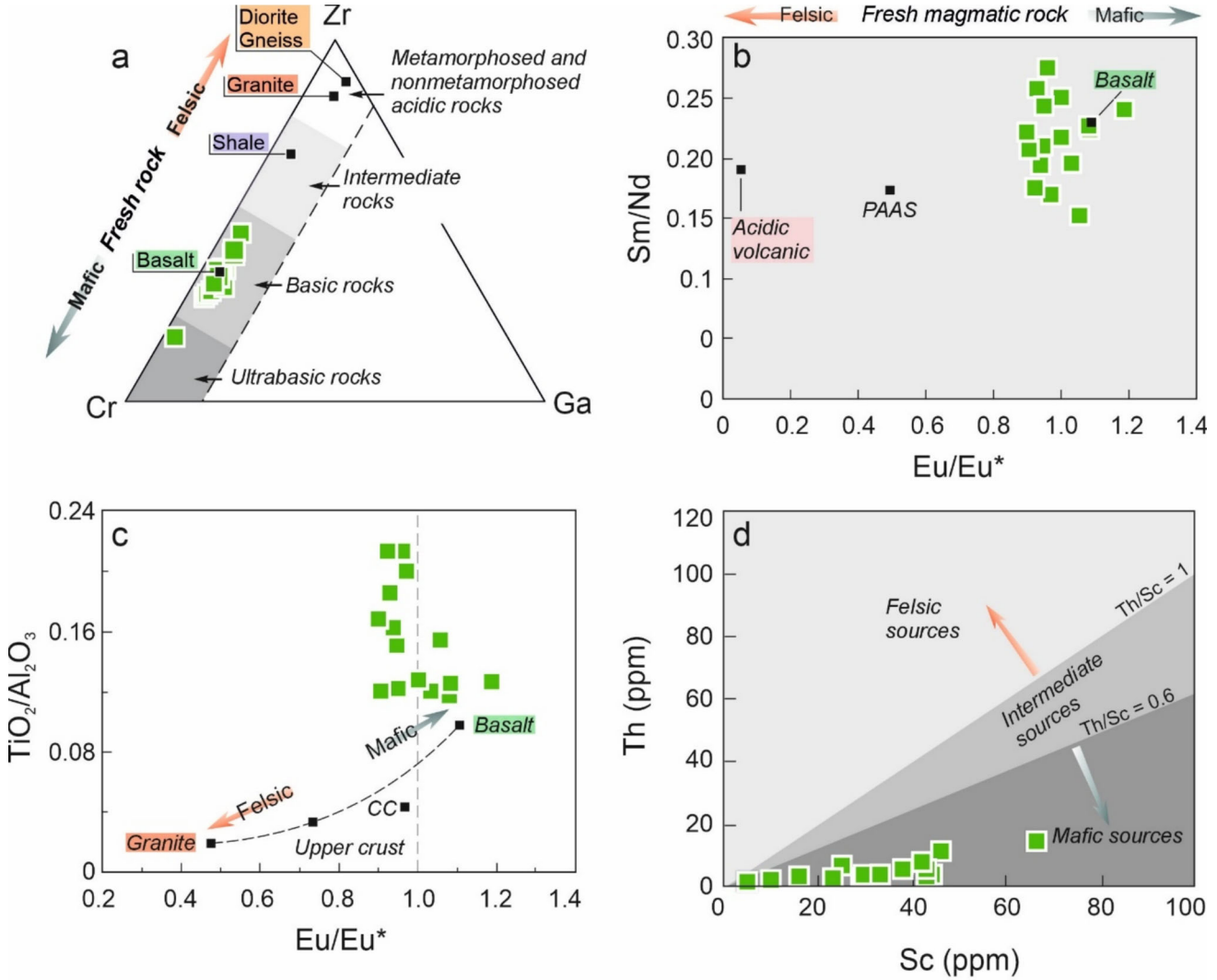

Fig. 11 **a** Ga-Zr-Cr ternary plot showing ultrabasic, basic, intermediate and acidic parent rocks (reference rock analyses from USGS), **b** Sm/Nd vs Eu/Eu* binary plot showing average standard rock lithologies. **c** Eu/Eu* vs TiO_2/Al_2O_3 binary plot showing the bauxite geochemical signature to be closely related to basalt, **d** Th vs Sc diagram showing field of felsic, intermediate and mafic sources

to study rock weathering and REE mobilisation in soils [124]. It is well known that Th and La are enriched in acidic rocks, whereas Sc has high concentrations in mafic rocks, and Cr is an immobile element enriched in ultrabasic rocks. Th vs Sc diagram shows in mafic sources for studied lateritic bauxites (Fig. 11D).

A new schematic diagram was proposed by Piovano et al. [125] to identify the source areas of metamorphic rocks, granitic rocks and sediments from the Eastern Sierras Pampeanas (Argentina). In this diagram, the ratio of four immobile elements (Cr, La, Sc, Th) to each other (Th/Sc vs La/Cr) was used (Fig. 12). Although this diagram was designed to determine the origins of sediments, it also helped to reveal the origins of bauxite deposits. Rocks with an acidic character are plotted in the upper-right part of the diagram, while rocks with basic and ultrabasic compositions cluster in the lower-left part. Rocks of intermediate composition fall in the central part of the diagram. The present study uses geochemical data (e.g. Th, Sc, La, Cr) from comprehensive bauxite studies reported in the literature. These data were then compared with the results of this study to define the probable parent rocks (acidic, intermediate, basic and ultrabasic sources) based on this diagram. In addition, international standard references (USGS, LC, CC, UCC, [126]) for rock analyses ranging from acidic to basic are included. This conclusion aligns well with the Th/Sc and La/Cr bivariate diagram (Fig. 12) tested to discriminate the likely source rocks of bauxites. The four groups of sources

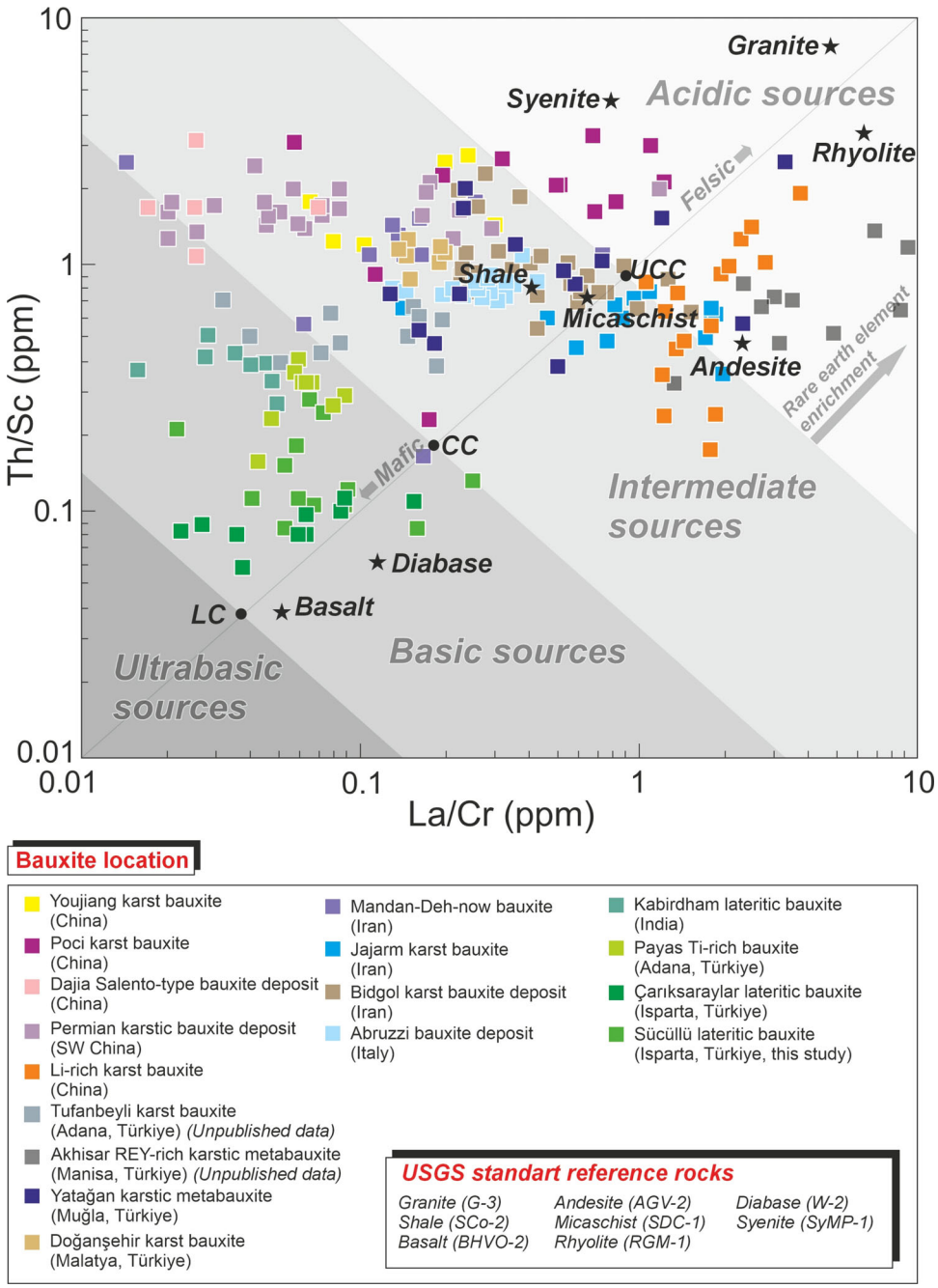

Fig. 12 Th/Sc vs La/Cr diagram illustrating domains of ultrabasic, basic, intermediate and acidic sources in locations of different bauxite deposits around the world [modified after from 125] UCC: Upper Continental Crust, CC: Continental Crust, LC: Lower Crust [126]. *Note:* standard reference rocks are from the USGS. Data for bauxite deposits [36, 49, 52, 113, 127–134]

are illustrated by a plot of Th/Sc vs. La/Cr. In this diagram, lateritic occurrences and bauxite deposits with low La/Cr and Th/Sc values are plotted in the lower-left part, while high values are found in the upper-right part. La/Cr and Th/Sc values of karstic bauxite deposits from around the world have an intermediate composition and fall in the central part of the diagram. Specifically, high values of Th/Sc and La/Cr in the Li-rich karst bauxite (China), Poci karst bauxite (China) and regionally metamorphosed REY-rich karstic bauxite deposits of Akhisar (Manisa region, Türkiye) indicate strongly acidic nature, slightly intermediate precursor. On this diagram, Ti-rich bauxites (Payas, Çarıksaraylar, Sücüllü, Kabirdham) also have a basic composition. Overall, discriminant diagrams based on immobile element suggest that lateritic bauxite deposits from the Sücüllü region are derived from a basic precursor, specifically alkali doleritic basalt.

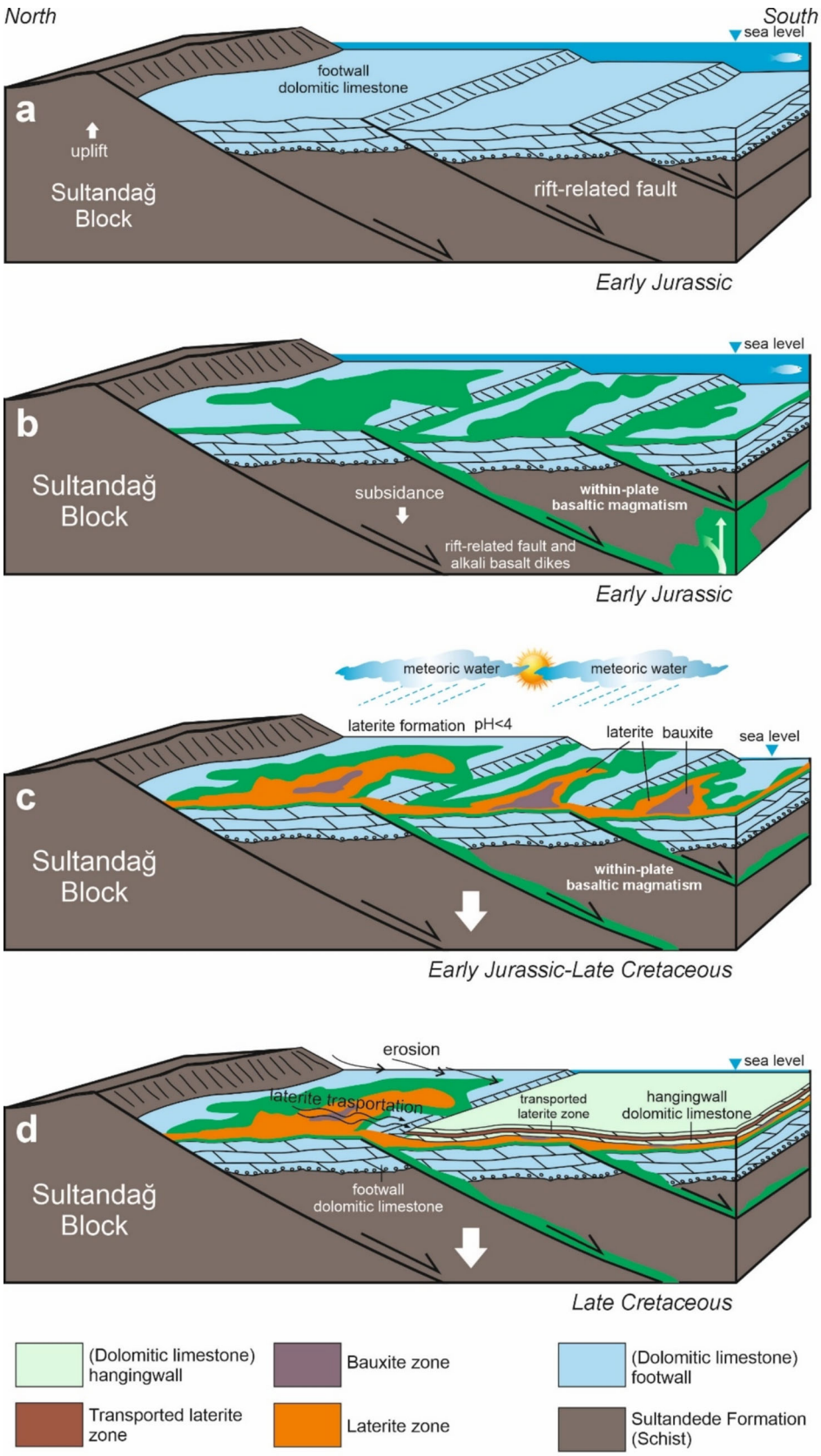

Fig. 13 Tectonic diagram showing formation of the Sücüllü lateritic bauxite deposits in Tauride belt (southern Türkiye). **a** Precipitation of dolomitic limestones (Hacıalabaz limestone), uplift of Sultandağ Block with rift-related normal fault systems, **b** within-plate submarine alkali basaltic magmatism along rift-related normal faults, **c** laterite and bauxite formation on the alkali basalt rocks in terrestrial environment, **d** transportation on the dolomite of lateritic bauxite deposits on land

7.3 Tectonic Model

It has been shown that the Jurassic Period provides a valuable record of tectonic setting, palaeo-environment and climatic change in continental configuration, extending from 201.3 to 145.0 Ma [135]. During the late Early and Middle Jurassic (180–155 Ma), the climate was extremely hot at low latitudes. Mean sea surface temperatures at the equator were over 30 °C. Despite the fact that the global average temperature was about 6–9 °C higher than today, sea levels were generally high during the Jurassic. The Cretaceous was much warmer than the Jurassic. During the Late Cretaceous, the southern part of Turkey was located around 20.°N latitude and the average surface temperature of the sea water was between 20 and 25 °C during that period [136, 137]. At that time, intense weathering resulted in the formation of large lateritic bauxite deposits in eastern Mediterranean domains [36]. Their stratigraphic position and geochemical signature are of great importance in answering the questions related to the evolutionary history of the tectonics of the Taurid orogenic belt in the eastern Mediterranean region. In Anatolia, the distribution of bauxites is closely linked to the development of the Neo-Tethys realm. In terms of tectonic and geological evolution, the Mesozoic thick-bedded platform sequences of this orogenic belt are mostly represented by a passive continental margin [138]. The supercontinent of Pangea began to break apart and ocean basins separated into two megacontinents, Laurasia to the north and Gondwana to the south [139]. During the Late Permian to Early Middle Jurassic, the Neotethys Ocean opened as a consequence of significant NW–SE continental rifting of the Tauride-Anatolian Plate from the northern margin of Gondwana [75, 140–143]

During the Jurassic, platform-type carbonate sequences (Hacıalabaz limestone) were deposited along a south-facing passive continental margin. They began to break apart with significant NW–SE rifting (Fig. 13A). Along the normal faults associated with rifting, within-plate mafic magma (doleritic alkali basalt) ascended along the fault zones of the basement lithologies of the Sultandağ Block, spreading over the limestones deposited on the platform (Fig. 13B). The continent subsided, an intense inflow of mafic magma into the shallow marine environment occurred. A favourable environment for the lateritisation process was created by the terrestrial conditions that followed the shallow marine environment during the Jurassic. With tectonic mobility along normal faults, basaltic rocks remaining in the terrestrial environment began to form lateritic zones under acidic pH (< 4) conditions. From Early Jurassic to Late Cretaceous, the ongoing acidic environment leached basaltic rocks in the terrestrial environment (Fig. 13C), and bauxite formed in situ as a result of the lateritisation process. With continued tectonic movements and changes in sea level, the lateritic bauxite zones formed in the terrestrial environment were transported into the sea over dolomites (Fig. 13D). The succession of very thin dolomitic limestones and lateritic soils in the studied area reflects that the transport event occurred multiple times.

Our preferred interpretation is that there was a transition from marine to terrestrial conditions in the hot climate period of Upper Cretaceous. The doleritic alkali basalt overlying the limestone was weathered to bauxite under this conditions (Fig. 13C). Öztürk et al. [36] point out that isotopic data (oxygen, carbon) from the footwall and hanging-wall limestones in the Payas (southern Turkey) region indicate a transition from hot to a cold climate. Consequently, laterites and bauxites in terrestrial environment were eroded and transported over the dolomitic limestone. Additionally, dolomitic limestones were re-deposited on the lateritic soil.

The deposition of platform-type carbonates, which began to form in a passive continental margin of the Neo-Tethys Ocean, occurred mainly between the Late Triassic and Late Cretaceous. A recent study [144] noted that the age of the alkaline basalts is estimated to be 161.9 ± 10.6. These alkaline basalts, products of intracontinental (within-plate) volcanism, were distributed on the seafloor by cutting through the basement units, as well as on the dolomites deposited on the platform, immediately after the break-up of the Tauride platform with the onset of the rifting mechanism [137]. According to Haude [145], the alkaline doleritic basalts hosting lateritic bauxite deposits in the region are the result of initial submarine volcanism formed by the rifting mechanism of the Tauride platform.

8 Conclusions

The study of the lateritic bauxite deposits in the western part of the Sultandağ Range (Sücüllü-Yalvaç, Isparta) indicated the following conclusions:

1. In situ lateritic bauxite deposits are found on Jurassic-aged submarine basaltic volcanic rocks, whereas transported laterites are found on thin-bedded dolomitic limestone, which is well exposed on the western slope of the Sultandağ Mountains.
2. Regionally, the lateritic bauxite horizon is associated with thicknesses ranging from 5 to 30 m (average 15 m) in a northwest–southeast direction across the region.
3. On the basis of the petrographical studies, altered volcanic rocks, which are the host rock of lateritic bauxites, have dominant mineral assemblages of plagioclase, clinopyroxene (augite) and also palagonite and chlorite as an alteration products. XRD and SEM studies suggest that the assemblages of the lateritic bauxites include kaolinite, smectite, hematite, calcite, anatase, boehmite,

diaspore, goethite, feldspar, cristobalite, quartz, calcite and dolomite.

4. In the present study, the geochemical compositions of the Sücüllü lateritic bauxites are compared with metamorphosed and unmetamorphosed karst bauxites and lateritic bauxite occurrences worldwide. Based on trace element geochemistry (Th, La, Sc, Cr contents), the nature of their protolith is consistent with basic volcanic rocks, similar to the Ti-rich bauxites (Payas, Adana) and Çarıksaraylar lateritic bauxites (Şarkikaraağaç, Isparta) in the Taurides of Turkey, and in the Darai-Daldali region of India.
5. Conclusively, the lateritic bauxite deposits in the Sücüllü area (Yalvaç, Isparta) were formed as a result of lateritisation under warm humid climate of submarine alkaline basaltic rocks on neritic dolomitic carbonate sequence of a passive continental margin of the Mesozoic Inner-Tauride Ocean.

Acknowledgements This study is a part of MSc thesis of Betül Çoşkun. Financial support was provided by a grant from the Research Foundation of Süleyman Demirel University, Türkiye (SDU; grant #: 2634-YL-11). We would like to thank Fatih Kocadere for his support in the fieldwork. The authors thank the Editor Bassam El Ali for their time and effort to provide feedback on our manuscript, and anonymous referees for their truly detailed and extremely helpful review.

References

1. Berthier, P.: Analyse de l'alumine hydrat´ee des Beaux, d´epartement des Bouchesdu-Rhone. Ann. Mines, 1st Ser. **6**, 531–534 (1821)
2. Patterson, S.; Kurtz, H.; Olson, J.; Neeley, C.: World bauxite resources, geology and resources of aluminium. US Geological Survey professional paper 1076-B (1986)
3. Bárdossy, G.Y.; Aleva, G.J.J.: Lateritic Bauxites: Developments in Economic Geology, Vol. 27, p. 624. Elsevier, Amsterdam (1990)
4. Mondillo, N.; Balassone, G.; Boni, M.; Rollinson, G.: Karst bauxites in the Campania Apennines (southern Italy): a new approach. Per. Mineral. **80**, 407–432 (2011). https://doi.org/10.2451/2011PM0028
5. Abedini, A.; Calagari, A.A.: REE geochemical characteristics of titanium-rich bauxites: the Permian Kanigorgeh horizon, NW Iran. Turk. J. Earth Sci. **5**, 513–532 (2014). https://doi.org/10.3906/yer-1404-11
6. Mongelli, G.; Buccione, R.; Gueguen, E.; Langone, A.; Sinisi, R.: Geochemistry of the Apulian allochthonous karst bauxite, Southern Italy: distribution of critical elements and constraints on late Cretaceous Peri-Tethyan palaeogeography. Ore Geol. Rev. **77**, 246–259 (2016). https://doi.org/10.1016/j.oregeorev.2016.03.002
7. Weng, S.; Yu, W.; Algeo, T.J.; Du, Y.; Li, P.; Lei, Z.; Zhao, S.: Giant bauxite deposits of South China: multistage formation linked to Late Paleozoic Ice Age (LPIA) eustatic fluctuations. Ore Geol. Rev. **104**, 1–13 (2019). https://doi.org/10.1016/j.oregeorev.2018.10.014
8. Bárdossy, G.: Karst bauxites: bauxite deposits on carbonate rocks. In: Developments in Economic Geology, Vol. 14, pp. 1–441
9. Calagari, A.A.; Abedini, A.: Geochemical investigations on Permo-Triassic bauxite horizon at Kanisheeteh, east of Bukan, West-Azarbaidjan, Iran. J. Geochem. Explor. **94**, 1–18 (2007). https://doi.org/10.1016/j.gexplo.2007.04.003
10. Deng, J.; Wang, Q.; Yang, S.; Liu, X.; Zhang, Q.; Yang, L.; Yang, Y.: Genetic relationship between the Emeishan plume and the bauxite deposits in Western Guangxi, China: constraints from U-Pb and Lu-Hf isotopes of the detrital zircons in bauxite ores. J. Asian Earth Sci. **37**, 412–424 (2010). https://doi.org/10.1016/j.jseaes.2009.10.005
11. MacLean, W.; Bonavia, F.; Sanna, G.: Argillite debris converted to bauxite during karst weathering: evidence from immobile element geochemistry at the Olmedo Deposit, Sardinia. Mineral. Deposita **32**, 607–616 (1997). https://doi.org/10.1007/s001260050126
12. Mameli, P.; Mongelli, G.; Oggiano, G.; Dinelli, E.: Geological, geochemical and mineralogical features of some bauxite deposits from Nurra (western Sardinia, Italy): insights on conditions of formation and parental affinity. Int. J. Earth Sci. **96**, 887–902 (2007). https://doi.org/10.1007/s00531-006-0142-2
13. Pajović, M.: Genetic model of the karstic bauxites in the dinarides. In: Karamata S, Jankovic S (Eds.) Proceedings of the International Symposium Geology and Metallogeny of the Dinarides and the Vardar Zone. Academy of Sciences and Arts of The Republic of Srpska, Banja Luka, p 537 (2000)
14. Pajović, M.: Genesis and genetic types of karst bauxites. Iran. J. Earth Sci. **1**, 44–56 (2009)
15. Radusinovic, S.; Jelenkovic, R.; Pacevski, A.; Simic, V.; Bozovic, D.; Holclajtner-Antunovic, I.; Zivotic, D.: Content and mode of occurrences of rare earth elements in the Zagrad karstic bauxite deposit (Nikšic area, Montenegro). Ore Geol. Rev. **80**, 406–428 (2017). https://doi.org/10.1016/j.oregeorev.2016.05.026
16. Zarasvandi, A.; Charchi, A.; Carranza, E.J.M.: Karst bauxite deposits in the Zagros Mountain belt, Iran. Ore Geol. Rev. **34**, 521–532 (2008). https://doi.org/10.1016/j.oregeorev.2008.05.005
17. Zarasvandi, A.; Carranza, E.J.M.; Ellahi, S.S.: Geological, geochemical, and mineralogical characteristics of the and Deh-now bauxite deposits, Zagros Fold Belt. Iran. Ore Geol. Rev. **48**, 125–138 (2012). https://doi.org/10.1016/j.oregeorev.2012.02.010
18. Chen, J.; Wang, Q.; Zhang, Q.; Carranza, E.J.M.; Wang, J.: Mineralogical and geochemical investigations on the iron-rich gibbsitic bauxite in Yongjiang basin, SW China. J. Geochem. Explor. **188**, 413–426 (2018). https://doi.org/10.1016/j.gexplo.2018.02.007
19. Gow, N.N.; Lozej, G.P.: Bauxite. Geosci. Can. **20**, 9–16 (1993)
20. Madourie, M.: A comparative analysis between Portuguese and Jamaican bauxite rocks: their geo-economic potential for the aluminum industry. Master's Thesis, Faculty of Sciences, University of Porto, Portugal. pp. 82 (2013)
21. Bogatyrev, B.A.; Zhukov, V.V.: Bauxite provinces of the world. Geol. Ore Dep. **51**, 339–355 (2009). https://doi.org/10.1134/S1075701509050018
22. Mongelli, G.; Acquafredda, P.: Ferruginous concretions in a Late Cretaceous karst bauxite: composition and conditions of formation. Chem. Geol. **158**, 315–320 (1999). https://doi.org/10.1016/S0009-2541(99)00061-3
23. Bárdossy, G.: Carboniferous to Jurassic bauxite deposits as paleoclimatic and paleogeographic indicators. In: Embry, A.F., Beauchamp, B., Glass, D.J. (eds.) Pangea: Global Environments and Resources. Canadian Society of Petroleum Geologists Memoir, pp. 283–293 (1994)
24. Özlü, N.: Trace-element content of "Karst Bauxites" and their parent rocks in the Mediterranean Belt. Miner. Deposita **18**(3), 469–476 (1983). https://doi.org/10.1007/BF00204491
25. Ayhan, A.; Karadağ, M.M.: Şarkikaraağaç (Isparta) güneyinde bulunan boksitli demir ve demirli boksit yataklarının jeolojisi ve oluşumu [Geology and origin of bauxitic iron and ferruginous bauxite deposits in the South of Şarkikaraağaç (Isparta)]. Bull. Geol. Soc. Turk. **28**, 137–146 (1985) (**in Turkish with English abstract**)

26. Cengiz, O.: Şarkikaraağaç (Isparta) ve Hüyük-Doğanhisar (Konya) arasındaki barit yatakları ve oluşumu. Süleyman Demirel Üniversitesi, Fen Bilimleri Enstitüsü, Doktora Tezi, 247 s. (in Turkish with English abstract) (1997)
27. Öztürk, H.; Hein, J.R.; Hanilçi, N.: Genesis of the Doğankuzu and Mortaş bauxite deposits, Taurides, Turkey: separation of Al, Fe, and Mn and implications for passive margin metallogeny. Econ. Geol. **97**, 1063–1077 (2002). https://doi.org/10.2113/gsecongeo.97.5.1063
28. Karadağ, M.; Küpeli, S.; Arık, F.; Ayhan, A.; Zedef, V.; Döyen, V.: Rare earth element (REE) geochemistry and genetic implications of the Mortas bauxite deposit (Seydişehir/Konya–Southern Turkey). Chem. Erde **69**, 143–159 (2009). https://doi.org/10.1016/j.chemer.2008.04.005
29. Hanilçi, N.: Geological and geochemical evolution of the Bolkardağı bauxite deposits, Karaman, Turkey: transformation from shale to bauxite. J. Geochem. Explor. **133**, 118–137 (2013). https://doi.org/10.1016/j.gexplo.2013.04.004
30. Hanilçi, N.: Bauxite deposits of Turkey. In: Pirajno, F.; Ünlü, T.; Dönmez, C.; Şahin, M.B. (Eds.) Mineral Resources of Turkey. Modern Approaches in Solid Earth Sciences, Vol. 16, pp. 681–730. Springer, Berlin (2019)
31. Hanilçi, N.; Öztürk, H.; Kasapçı, C.: Carbonate-Hosted Pb-Zn Deposits of Turkey. In: Pirajno, F.; Ünlü, T.; Dönmez, C.; Şahin, M.B. (Eds.) Mineral Resources of Turkey. Modern Approaches in Solid Earth Sciences, Vol. 16, pp. 497–533. Springer, Berlin (2019)
32. Chaikin, L.; Shoppert, A.; Valeev, D.; Loginova, I.; Napol'skikh, J.: Concentration of rare earth elements (Sc, Y, La, Ce, Nd, Sm) in bauxite residue (red mud) obtained by water and alkali leaching of bauxite sintering dust. Minerals **10**, 500 (2020). https://doi.org/10.3390/min10060500
33. Singh, U.; Thawrani, S.A.; Agnihotr, A.: Rare earth elements recovery from red mud. The chapter is from the book Environmental Technologies to Treat Rare Earth Elements (2022)
34. Arslan, S.; Demir, G.K.; Celikel, B.; Baygul, M.; Suarez, C.E.: ETI Aluminum Red Mud Characterization and Processing. Light Metals, Edited by: Carlos E. Suarez TMS (The Minerals, Metals and Materials Society) (2012)
35. Öztürk, H.; Cansu, Z.; Kasapçı, C.; Hanilçi, N.; Banks, D.: REE and trace element mobility during the transformation of basalt to laterite and bauxite, Payas Province, Türkiye. Geochemistry **4**, 126083 (2024). https://doi.org/10.1016/j.chemer.2024.126083
36. Öztürk, H.; Hanilçi, N.; Cansu, Z.; Kasapçı, C.: Formation of Ti-rich bauxite from alkali basalt in continental margin carbonates, Payas region, SE Turkey: implications for sea level change in the Upper Cretaceous. Turk. J. Earth Sci. **30**, 116–141 (2021). https://doi.org/10.3906/yer-2006-6
37. Hajikazemi, E.; Al-Aasm, I.S.; Coniglio, M.: Diagenetic history and reservoir properties of the Cenomanian-Turonian carbonates in southwestern Iran and the Persian Gulf. Mar. Pet. Geol. **88**, 845–857 (2017). https://doi.org/10.1016/j.marpetgeo.2017.06.035
38. Ahmadnejad, F.; Mongelli, G.: Geochemistry of upper Cretaceous bauxite deposits, Zagros Fold Thrust Belt, SW Iran: paleoenvironment and provenance constraints. Sediment. Geol. **454**, 106461 (2023). https://doi.org/10.1016/j.sedgeo.2023.106461
39. Şengör, A.M.C.; Yılmaz, Y.: Tethyan evolution of Turkey: a plate tectonic approach. Tectonophysics **75**, 81–241 (1981). https://doi.org/10.1016/0040-1951(81)90275-4
40. Robertson, A.H.F.; Dixon, J.E.: Introduction: aspects of the geological evolution of the Eastern Mediterranean. In: Dixon, J.E., Robertson, A.H.F. (Eds.) The Geological Evolution of the Eastern Mediterranean, Geological Society Special Publication, Vol. 17, pp. 1–74 (1984)
41. Okay, A.I.: Was the late Triassic orogeny in Turkey caused by the collision of an oceanic plateau? Geol. Soc., Lond., Spec. Publ. **173**, 25–41 (2000). https://doi.org/10.1144/GSL.SP.2000.173.01.02
42. Bağcı, U.; Rızaoğlu, T.; Önal, G.; Parlak, O.: Petrology of the late Triassic mafic volcanic rocks from the Antalya Complex, southern Turkey: evidence for mantle source characteristics during the Neotethyan rifting: Turk. J. Earth Sci. **29**, 1049–1072 (2020). https://doi.org/10.3906/yer-2003-1
43. Nicolas, J.; Özlü, N.: Contribution AL'etude De Gisement De Bauxite De Kiziltas Dans Les Taurides Occidentales (Turquie Meridionale). Comptes Rendus de l'Académie des Sciences Serie D **282**(0013), 1253–1255 (1976) (**in French**)
44. Özlü, N.: Different modes of formation of bauxite breccia in bauxite deposits of Western Taurides (Southern Turkey). Comptes Rendus Hebdomadaires des Seances De L Academie des Sciences Serie D **284**, 1021–1023 (1977)
45. Özlü, N.: Etude geologique, mineralogique et geochim- ique des bauxites de la region d'Akseki-Seydisehir (Taurus occidental-Turquie): Paris, Pierre et Marie Curie Universite, Doctoral dissertation, 455 p. (1978)
46. Temur, S.; Orhan, H.; Deli, A.; Karadağ, M. M.: The soil chemistry in Tinaztepe Cave (Seydişehir-Konya) and its environ and the relations of similar soils with bauxites; Selçuk Univ. Sci. Found. Project, 102 p (In Turkish) (2005)
47. Temur, S.; Kansun, G.: Geology and petrography of the Masatdagi diasporic bauxites, Alanya, Antalya, Turkey. J. Asian Earth Sci. **27**, 512–522 (2006). https://doi.org/10.1016/j.jseaes.2005.07.001
48. Hatipoğlu, M.; Helvacı, C.; Chemberlain, S.C.; Babalık, H.: Mineralogical characteristics of unusual 'Anatolian' diaspore (zultanite) crystals from the Ilbirdağı diasporite deposit, Turkey. J. Afr. Earth Sci. **57**, 525–541 (2010). https://doi.org/10.1016/j.jafrearsci.2010.01.002
49. Aydoğan, M.S.; Moazzen, M.: Origin and metamorphism of corundum-rich metabauxites at Mt. Ismail in the Southern Menderes Massif, SW Turkey. Resour. Geol. **3**, 243–262 (2012). https://doi.org/10.1111/j.1751-3928.2012.00193.x
50. Yalçın, M.G.; İlhan, S.: Major and trace element geochemistry of bauxites of Ayranci, Karaman, Central Bolkardag, Turkey. Asian J. Chem. **5**, 2893–2904 (2013). https://doi.org/10.14233/ajchem.2013.14275
51. Gündoğan, İ: Meta-bauxite deposit in the Tavşanlı Zone, NW Turkey: a new locality for gem-quality diaspore formation. J. Asian Earth Sci. **8**, 100114 (2022). https://doi.org/10.1016/j.jaesx.2022.100114
52. Bozkır, Y.: Çarıksaraylar ile Kozlucay (Şarkikaraağaç-Isparta) arasındaki boksitlerin NTE'leri ve oluşum şartları. MSc thesis, Selcuk University, Konya, Turkey (in Turkish with English abstract) (2007)
53. Coşkun, B.: Sücüllü (Yalvaç-Isparta) Lateritik Fe ve Al Oluşumlarının Jeolojik, Mineralojik ve Jeokimyasal Özellikleri ve Ekonomik Potansiyelinin Araştırılması. Sülayman Demirel Üniversitesi, Fen Bilimleri Enstitüsü, Yüksek Lisans Tezi, 86 s. (2012)
54. Öncel, M.S.: Şarkikaraağaç-Yalvaç (Isparta) arasının jeolojisi ve boksit zuhurlarının mineralojik, petrografik, jeokimyasal incelemesi [Geology of Şarkikaraağaç-Yalvaç (Isparta) and mineralogical, petrographical, geochemical investigation of bauxite occurrences]. PhD thesis Selçuk University. p 147. (in Turkish, unpublished) (1995)
55. Zitter, T.A.; Woodside, J.M.; Mascle, J.: The Anaximander mountains: a clue to the tectonics of southwest Anatolia. Geol. J. **38**, 375–394 (2003). https://doi.org/10.1002/gj.961
56. Özgül, N.: Some geological aspects of the Taurus orogenic belt. Geol. Bul. Turkey **19**, 65–78 (1976)

57. Koçyiğit, A.: Hoyran Gölü (Isparta Büklümü) dolayının tektoniği. Türkiye Jeoloji Bülteni **26**, 1–10 (1983)
58. Özgül, N.; Turşucu, A.: Stratigraphy of the Mesozoic carbonate sequence of the Munzur Mauntains (Eastern Taurides). In: Tekeli, O.; Göncüoğlu, M.C. (Eds.) Geology of the Taurus Belt, Ankara, pp. 173–181 (1984)
59. Tekeli, O.; Aksay, A.; Ürgün, B.; Işık, A.: Geology of the Aladağ Mountains. In: Tekeli, O.; Göncüoğlu M.C. (Eds.) Geology of the Taurus Belt, Proceedings of the International Symposium on the Geology of the Taurus Belt. Miner. Res. Explor. Inst. Turkey. Spec. Publ., pp. 143–158 (1984)
60. Şenel, M.: Discussion on the Antalya nappes. In: Tekeli, O.; Göncüoğlu, M.C. (Eds.) Geology of the Taurus Belt, Int. Sym. 26–29 Sep. 41–52 (1984)
61. Demirtaşlı, E.; Turhan, N.; Bilgin, A.Z.; Selim, M.: Geology of the Bolkar Mountains. In: Tekeli, O.; Göncüoğlu, M.C. (Eds.) Geology of the Taurus Belt Proceedings International Symposium on the Geology of the Taurus Belt, pp. 125–142. Ankara, MTA (1984)
62. Dilek, Y.; Rowland, J.C.: Evolution of a conjugate passive margin pair in Mesozoic southern Turkey. Tectonics **12**, 954–970 (1993). https://doi.org/10.1029/93TC01060
63. Polat, A.; Casey, J.F.: A structural record of the emplacement of the Pozanti-Karsanti ophiolite onto the Menderes-Taurus block in the late Cretaceous, eastern Taurides, Turkey. J. Struct. Geol. **12**, 1673–1688 (1995). https://doi.org/10.1016/0191-8141(95)00061-H
64. Özgül, N.: The stratigraphy of the lithology located in Bozkir–Hadim–Taskent (Northern Central Taurides). Bull. Miner. Res. Explor. Inst. Turk. **119**, 113–174 (1997) (**In Turkish**)
65. Andrew, T.; Robertson, A.H.F.: The Beyşehir–Hoyran–Hadim Nappes: genesis and emplacement of Mesozoic marginal and oceanic units of the northern Neotethys in southern Turkey. J. Geol. Soc. London **159**, 529–543 (2002). https://doi.org/10.1144/0016-764901-157
66. Collins, A.S.; Robertson, A.H.F.: Kinematic evidence for late Mesozoic-Miocene emplacement of the Lycian Allochthon over the western Anatolide Belt, SW Turkey. Geol. J. **38**, 295–310 (2003). https://doi.org/10.1002/gj.957
67. Brunn J.-H.; Dumont J.-F.; De Gracıansky P.-C.; Gutnıc M.; Juteau T.; Marcoux J.; Monod O.; Poisson A.: Outline of the geology of the western Taurids. In: A.S. Campbell (Ed.) Geology and history of Turkey. Tripoli, Petroleum Exploration Society of Lybia (1971)
68. Gutnic, M.; Monod, O.; Poisson, A.; Dumont, J.-F.: Géologie des Taurides occidentales (Turquie). Mém. Soc. géol. Fr. **137**, 1–112 (1979)
69. Robertson, A.H.F.: Mesozoic-tertiary sedimentary and tectonic evolution of Neo-Tethyan carbonate platform margins and small ocean basin in the Antalya complex of SW Turkey. Spec. Publ. Int. Assoc. Sedimentol. **20**, 127–146 (1993)
70. Dercourt, J.; Gaetani, M.; Vrielynck, B.; Barrier, E.; Biju-Duval, B.; Brunet, M.-F.; Cadet, J.-P.; Crasquin, S.; Sandulescu, M.: Atlas peri-tethys and explanatory notes, p. 268. CCGM, Paris (2000)
71. Poisson, A.; Yağmurlu, F.; Bozcu, M.; Sentürk, M.: New insights on the tectonic setting and evolution around the apex of the Isparta angle (SW Turkey). Geol. J. **38**, 257–282 (2003). https://doi.org/10.1002/gj.955
72. Poisson, A.; Orszag-Sperber, F.; Kosun, E.; Basietti, M.-A.; Müller, C.; Wernli, R.; Rouchy, J.-M.: The Late Cenozoic evolution of the Aksu basin (Isparta Angle; SW Turkey). New Insights. Bull. Soc. Géol. Fr. **182**(2), 133–148 (2011). https://doi.org/10.2113/gssgfbull.182.2.133
73. Elitok, Ö.: Geochemistry and tectonic significance of the Şarkikaraağaç Ophiolite in the Beyşehir–Hoyran Nappes, SW Turkey. In: Proceedings of the 4th International Symposium on Eastern Mediterranean Geology, pp. 181–196 (2001)
74. Elitok, Ö.; Drüppel, K.: Geochemistry and tectonic significance of metamorphic sole rocks beneath the Beyşehir-Hoyran ophiolite (SW-Turkey). Lithos **100**, 322–353 (2008). https://doi.org/10.1016/j.lithos.2007.06.022
75. Robertson, A.H.F.; Ustaömer, T.; Pickett, E.A.: Testing models of Late Palaeozoic-Early Mesozoic orogeny in Western Turkey: Support for an evolving open-Tethys model. J. Geol. Soc. **3**, 501–511 (2004). https://doi.org/10.1144/0016-764903-080
76. Blumental, M.M.: Seydişehir-Beyşehir hinterlandındaki Toros dağlarının jeolojisi. MTA Yayınları **2**, 242–252 (1947)
77. Dumont, J.F.: Les deux types de soubbassements paléozoiques dans la coupole de Karacahisar (région d'Isparta, Turquie) et leur séparation par un accident anté-triassique: Bull. Miner. Res. Explor. **90**, 77–81 (1978)
78. Poisson, A.: Récherches Géologiques dans les Taurides Occidentales, Turquie. (PhD Thesis). Université de Paris-Sud, Orsay, France (1977)
79. Glover, C.; Robertson, A.: Neotectonic intersection of the Aegean and Cyprus tectonic arcs: extensional and strike-slip faulting in the Isparta Angle, SW Turkey. Tectonophysics **298**, 103–132 (1998). https://doi.org/10.1016/S0040-1951(98)00180-2
80. Piper, J.D.A.; Gürsoy, H.; Tatar, O.; İşseven, T.; Koçyiğit, A.: Paleomagnetic evidence for the Gondwanic origin of the Taurides and rotation of the Isparta Angle, southern Turkey. Geol. J. **37**, 317–336 (2002). https://doi.org/10.1002/gj.920
81. Koçyiğit, A.; Özacar, A.A.: Extensional neotectonic regime through the NE edge of the outer Isparta Angle, SW Turkey: new field and seismic data. Turk. J. Earth Sci. **12**, 67–90 (2003)
82. Dean, V.T.; Monod, O.: The lower Paleozoic stratigraphy and faunas of the Taurus Mountains near Beyşehir, Turkey. I. Stratigraphy Bull. Brit. Mus. Nat. Hist. Geol. **8**, 411–426 (1970)
83. Demirkol, C.; Sipahi, H.: Bağkonak-Çimendere Muratdağı (Isparta) Yöresinin Jeolojisi. Jeoloji Mühendisliği Dergisi, 29–36 s. (in Turkish with English abstract) (1979)
84. Elmas, N.: Dinek (Şarkikaraağaç-Isparta) ve çevresindeki barit cevherleşmeleri. İstanbul Teknik Üniversitesi, Fen Bilimleri Enstitüsü, Doktora Tezi, 102 s. (2005)
85. Cengiz, O.; Kuşçu, M.: Şarkikaraağaç Isparta ile Hüyük Konya arasındaki barit yataklarının jeokimyasal özellikleri ve kökeni. Maden Tetkik Arama Derg. **123**, 67–89 (2002)
86. Özgül, N.; Gedik, İ: New data on the stratigraphy and the conodont faunas of Çaltepe limestone and Seydişehir formation lower Paleozoic of central taurus range. Geol. Bull. Turkey **2**, 39–52 (1973)
87. Turan, A.: Akören (Konya, Orta Toroslar) Çevresinin Jeolojik Özellikleri. Selçuk Üniversitesi, Mühendislik-Mimarlık Fakültesi Dergisi **4**, 17–36 (2010) (**in Turkish with English abstract**)
88. Eren, Y.: Engilli (Akşehir)-Bağkonak (Yalvaç) köyleri arasında Sultandağlan Masifi'nin stratigrafisi: Ç.Ü., A.Acar Sempozyumu, Adana, pp. 83–92 (in Turkish with English abstract) (1990)
89. Nalbantçılar, M.T.: Çay (Afyon) güneybatısında Sultandağları Masifi'nin mesoskopik tektonik özellikleri ve jeoloji evrimi. Türkiye Jeoloji Bülteni **2**, 17–28 (1997) (**in Turkish with English abstract**)
90. Nalbantçılar, M.T.: Akkanok (Afyon)-Sağır (Isparta) arasında Sultandağları Masifi'nin tektonostratigrafisi: KTÜ Jeoloji Müh. Böl. 30. yıl sempozyumu bild., Trabzon, pp. 708–717 (1996)
91. Winchester, J.A.; Floyd, P.A.: Geochemical discrimination of different magma series and their differentiation products using immobile elements. Chem. Geol. **20**, 325–343 (1977). https://doi.org/10.1016/0009-2541(77)90057-2
92. Pearce, J.: Sources and settings of granitic rocks. Episodes **19**, 120–125 (1996). https://doi.org/10.18814/epiiugs/1996/v19i4/005

93. Aleva, G.J.J.: Laterites: Concepts, Geology, Morphology and Chemistry. In: International Soil Reference and Information Center (ISRIC) (ed.) The Corlat Handbook, Corlat Technical Publication, Brussels, pp. 8–21 (1994)
94. Ma, L.; Jin, L.; Brantley, S.L.: How mineralogy and slope aspect aAect REE release and fractionation during shale weathering in the Susquehanna/Shale Hills Critical Zone Observatory. Chem. Geol. **290**(1–2), 31–40 (2011). https://doi.org/10.1016/j.chemgeo.2011.08.013
95. Nesbitt, H.; Wilson, R.: Recent chemical weathering of basalts. Am. J. Sci. **292**, 740–777 (1992). https://doi.org/10.2475/ajs.292.10.740
96. Hayashi, K.I.; Fujisawa, H.; Holland, H.D.; Ohmoto, H.: Geochemistry of ∼1.9 Ga sedimentary rocks from northeastern Labrador, Canada. Geochim. Cosmochim. Acta **61**, 4115–4137 (1997). https://doi.org/10.1016/S0016-7037(97)00214-7
97. Wang, Z.; Li, Y.; Algeo, T.J.; Yu, W.; He, X.-F.: Critical metal enrichment in upper Carboniferous karst bauxite of North China Craton. Miner. Deposita **59**, 237–254 (2024). https://doi.org/10.1007/s00126-023-01207-6
98. Price, J.R.; Velbel, M.A.: Chemical weathering indices applied to weathering profiles developed on heterogeneous felsic metamorphic parent rocks. Chem. Geol. **202**(3–4), 397–416 (2003). https://doi.org/10.1016/j.chemgeo.2002.11.001
99. Nesbitt, H.W.; Young, G.M.: Early proterozoic climates and plate motions inferred from major element chemistry of lutites. Nature **299**, 715–717 (1982)
100. Nesbitt, H.W.; Young, G.M.: Prediction of some weathering trends of plutonic and volcanic rocks based on thermodynamic and kinetic considerations. Geochim. Cosmochim. Acta **48**(7), 1523–1534 (1984). https://doi.org/10.1016/0016-7037(84)90408-3
101. Falkum, T.; Grundvig, S.: Geochemical evidence in support of sedimentary precursors to Proterozoic sillimanite-bearing rocks, Vest-Agder, South Norway. NGU-BULL **446**, 19–34 (2006)
102. Trolard, F.; Tardy, Y.: The stabilities of gibbsite, boehmite, aluminous goethites and aluminous hematites in bauxites, ferricretes and laterites as a function of water activity, temperature and particle size. Geochim. Cosmochim. Acta **51**, 945–957 (1987). https://doi.org/10.1016/0016-7037(87)90107-4
103. Babechuk, M.G.; Widdowson, M.; Kamber, B.S.: Quantifying chemical weathering intensity and trace element release from two contrasting basalt profiles, Deccan Traps, India. Chem. Geol. **363**, 56–75 (2014). https://doi.org/10.1016/j.chemgeo.2013.10.027
104. Schellmann, W.: Considerations on the definition and classification of laterites, Proc. of the International seminar on lateritization processes, IGCP 129 and IAGC, Trivandrum, India, Oxford and IBH Publ. Co., New Delhi, pp. 1–10 (1981)
105. Schellmann, W.: A new definition of laterite; In: Lateritization Processes (ed.) Banerjee P K, Geol. Surv. India Memoir **120**, 1–7 (1986)
106. Ohta, T.; Arai, H.: Statistical empirical index of chemical weathering in igneous rocks: a new tool for evaluating the degree of weathering. Chem. Geol. **240**(3–4), 280–297 (2007). https://doi.org/10.1016/j.chemgeo.2007.02.017
107. Crnicki, J.; Jurkovic, I.: Rare earth elements in Triassic bauxites of Croatia Yugoslavia. Travaux **19**, 239–248 (1990)
108. Maksimovic, Z.; Panto, G.: Contribution to the geochemistry of the rare earth elements in the karst-bauxite deposits of Yugoslavia and Greece. Geoderma **51**(1–4), 93–109 (1991). https://doi.org/10.1016/0016-7061(91)90067-4
109. Bogatyrev, B.A.; Zhukov, V.V.; Tsekhovsky, Y.G.: Phanerozoic bauxite epochs. Geol. Ore Dep. **51**, 456–466 (2009). https://doi.org/10.1134/S1075701509060038
110. Ling, K.Y.; Tang, H.S.; Zhang, Z.W.; Wen, H.J.: Host minerals of Li–Ga–V–rare earth elements in Carboniferous karstic bauxites in southwest China. Ore Geol. Rev. **119**, 103325 (2020). https://doi.org/10.1016/j.oregeorev.2020.103325
111. D'Argenio, B.; Mindszenty, A.: Bauxites and related paleokarst: tectonic and climatic event markers at regional unconformities. Eclogae Geol. Helv. **88**, 453–499 (1995)
112. Bardossy, G.; Combes, P.J.: Karst bauxites: interfingering of deposition and palaeoweathering. Palaeoweathering, Palaeosurfaces and Related Continental Deposits, pp. 189–206 (1999)
113. Das, B.; Khan, M.W.Y.; Dhruw, H.: Trace and REE geochemistry of bauxite deposit of Darai-Daldali plateau, Kabirdham district, Chhattisgarh. India. J. Earth Syst. Sci. **129**, 117 (2020). https://doi.org/10.1007/s12040-020-1377-1
114. Ilijanić, N.; Kovačević Galović, E.; Gizdavec, N.; Ivkić Filipović, I.; Miko, S.; Peh, Z.: Geochemical records in subaerial exposure environments in Croatia using discriminant function analysis of bauxite data. Front. Earth Sci. **10**, 1055435 (2023). https://doi.org/10.3389/feart.2022.1055435
115. Yu, Q.; Jin, Y., Lu, S.; Ma, D.: Recent Research on Recovery of Iron and Aluminium from Bauxite Residue in China. TRAVAUX 53, Proceedings of the 42nd International ICSOBA Conference, Lyon, pp. 27–31 (2024)
116. Schroll, E.; Sauer, D.: Beitrage zur Geochemie von Titan, Chrom, Nickel, Cobalt, Vanadium und Molybdän in bauxitischen Gesteinen und das Problem der stofflichen Herkunft desAluminiums. Trav. ICSOBA **5**, 83–96 (1968)
117. Horbe, A.; Costa, M.: Geochemical evolution of a lateritic Sn–Zr–Th–Nb–Y–REEbearing ore body derived fromapogranite: the case of Pitinga, Amazonas-Brazil. J. Geochem. Explor. **66**(1–2), 339–351 (1999). https://doi.org/10.1016/S0375-6742(99)00002-3
118. Karadağ, M.M.: Seydişehir bölgesi boksitlerinin jeolojik, petrografik ve jenetik incelemesi. Doktora Tezi, Selçuk Üniversitesi, Fen Bilimleri Enstitüsü, 265 s. (yayımlanmamış) (1987)
119. Liu, X.M.; Rudnick, R.L.; McDonough, W.F.; Cummings, M.L.: Influence of chemical weathering on the composition of the continental crust: insights from Li and Nd isotopes in bauxite profiles developed on Columbia River basalts. Geochim. Cosmochim. Acta **115**, 73–91 (2013). https://doi.org/10.1016/j.gca.2013.03.043
120. Zamanian, H.; Ahmadnejad, F.; Zarasvandi, A.: Mineralogical and geochemical investigations of the Mombi bauxite deposit, Zagros Mountains, Iran. Geochemistry **76**, 13–37 (2016). https://doi.org/10.1016/j.chemer.2015.10.001
121. Mordberg, L.E.; Stanley, C.J.; Germann, K.: Mineralogy and geochemistry of trace elements in bauxites: the Devonian Schugorsk deposit, Russia. Mineral. Mag. **65**(1), 81–101 (2001). https://doi.org/10.1180/002646101550145
122. Gao, Z.X.; Liu, B.K.: Microstructure Study of Bauxite in China, p. 43. Metallurgy Industry Press, Beijing (2014).
123. Balasubramaniam, K.S.; Surendra, M.; Ravikumar, T.V.: Genesis of certain bauxite profiles from India. Chem. Geol. **60**, 227–235 (1987). https://doi.org/10.1016/0009-2541(87)90128-8
124. Viers, J.; Wasserburg, G.J.: Behavior of Sm and Nd in a lateritic soil profile. Geochim. Cosmochim. Acta **68**(9), 2043–2054 (2004). https://doi.org/10.1016/j.gca.2003.10.034
125. Piovano, E.L.; Ross, G.R.; Guevara, S.R.; Arribere, M.A.; Depetris, P.J.: Geochemical tracers of source rocks in a Cretaceous to Quaternary sedimentary sequence (Eastern Sierras Pampeanas, Argentina). J. South Am. Earth Sci. **12**(5), 489–500 (1999). https://doi.org/10.1016/S0895-9811(99)00031-0
126. Rudnick, R.; Gao, S.: Composition of the Continental Crust. In: Holland, H.D.; Turekian, K.K. (Eds.) Treatise on Geochemistry, pp. 1–64. Pergamon, Oxford (2003). https://doi.org/10.1016/B0-08-043751-6/03016-4
127. Yu, W.; Algeo, T.; Du, Y.; Zhang, Q.; Liang, Y.: Mixed volcanogenic–lithogenic sources for Permian bauxite deposits in

southwestern Youjiang Basin, South China, and their metallogenic significance. Sed. Geol. **341**, 276–288 (2016). https://doi.org/10.1016/j.sedgeo.2016.04.016
128. Yang, S.; Huang, Y.; Wang, Q.; Deng, J.; Liu, X.; Wang, J.: Mineralogical and geochemical features of karst bauxites from Poci (western Henan, China), implications for parental affinity and bauxitization. Ore Geol. Rev. **105**, 295–309 (2019). https://doi.org/10.1016/j.oregeorev.2018.12.028
129. Liu, X.; Wang, Q.; Deng, J.; Zhang, Q.; Sun, S.; Meng, J.: Mineralogical and geochemical investigations of the Dajia Salento-type bauxite deposits, western Guangxi, China. J. Geochem. Explor. **105**, 137–152 (2010). https://doi.org/10.1016/j.gexplo.2010.04.012
130. Hou, Y.; Zhang, Y.; Xu, Y.; He, B.: The provenance of late Permian karstic bauxite deposits in SW China, constrained by the geochemistry of interbedded clastic rocks, and U-Pb–Hf–O isotopes of detrital zircons. Lithos **278–281**, 240–254 (2017). https://doi.org/10.1016/j.lithos.2017.01.013
131. Zhao, H.; Wu, Z.; Zhang, S.; Zhou, X.; Wang, Y.; Cheng, H.: Geochemical features of lithium–rich bauxite from the Benxi Formation in Qinyuan County, Shanxi, China: insights into their depositional environment and lithium enrichment. Ore Geol. Rev. **163**, 105780 (2023). https://doi.org/10.1016/j.oregeorev.2023.105780
132. Ahmadnejad, F.; Zamanian, H.; Taghipour, B.; Zarasvandi, A.; Buccione, R.; Ellahi, S.S.: Mineralogical and geochemical evolution of the Bidgol bauxite deposit, Zagros Mountain Belt, Iran: implications for ore genesis, rare earth elements fractionation and parental affinity. Ore Geol. Rev. **86**, 755–783 (2017). https://doi.org/10.1016/j.oregeorev.2017.04.006
133. Putzolu, F.; Piccolo Papa, A.; Mondillo, N.; Boni, M.; Balassone, G.; Mormone, A.: Geochemical characterization of bauxite deposits from the Abruzzi Mining District (Italy). Minerals **8**(7), 298 (2018). https://doi.org/10.3390/min8070298
134. Kara, H.: Mineral signatures and trace and rare earth elements constraints on the sources of the Doğanşehir bauxite deposit (Malatya-Turkey). Geochem. Int. **61**(13), 1394–1412 (2023). https://doi.org/10.1134/S0016702923110058
135. Cohen, K.M.; Finney, S.C.; Gibbard, P.L.; Fan, J.-X.: The ICS International Chronostratigraphic Chart. Episodes **36**(3), 199–204 (2013). https://doi.org/10.18814/epiiugs/2013/v36i3/002
136. Kauffman, E.G.: Geological and biological overview: Western Interior Cretaceous Basin. In: Kauffman, E.G. (Ed.) Mountain Geologist. Rocky Mtn Assoc Geol **14**, 75–99 (1977)
137. Fritz, S.; Toth, T.A.: An Fe-berthierine from a Cretaceous laterite: Part II. estimation of Eh, pH and pCO_2 conditions of formation. Clays Clay Miner. **45**, 580–586 (1997). https://doi.org/10.1346/CCMN.1997.0450409
138. Collins, A.S.; Robertson, A.H.F.: Processs of Late Cretaceous to Late Miocene episodic thrust-sheet translation in the Lycian Taurides, SW Turkey. J. Geol. Soc. **155**, 759–772 (1998). https://doi.org/10.1144/gsjgs.155.5.075
139. Dera, G.; Prunier, J.; Smith, P.L.; Haggart, J.W.; Popov, E.; Guzhov, M.; Delsate, D.; Thies, D.; Cuny, G.; Puceat, E.; Charbonnier, G.; Bayon, G.: Nd isotope constraints on ocean circulation, paleoclimate, and continental drainage during the Jurassic breakup of Pangea. Gondwana Res. **27**(4), 1599–1615 (2015). https://doi.org/10.1016/j.gr.2014.02.006
140. Garfunkel, Z.: Constraints on the origin and history of the Eastern Mediterranean basin. Tectonophysics **298**(1–3), 5–35 (1998). https://doi.org/10.1016/S0040-1951(98)00176-0
141. Garfunkel, Z.: Origin of the Eastern Mediterranean basin: a reevaluation. Tectonophysics **391**, 11–34 (2004). https://doi.org/10.1016/j.tecto.2004.07.006
142. Gao, H.; Tong, X.; Wen, Z.; Wang, Z.: The tectonic evolution of the eastern Mediterranean basin and its control on hydrocarbon distribution. J. Pet. Eng. **178**, 389–407 (2019). https://doi.org/10.1016/j.petrol.2019.03.029
143. Gibbsons, A.D.; Whittaker, J.M.; Müller, R.D.: The breakup of East Gondwana: Assimilating constraints from Cretaceous ocean basins around India into a best-fit tectonic model. Solid Earth **118**, 808–822 (2013). https://doi.org/10.1002/jgrb.50079
144. Ergen, A.; Bozkurt, A.; Tuncay, E.; Ilgar, A.; Derinel, N.E.: Sultan Dağları'nda Jura bazik volkanizması: yeni yaş bulguları ve lateritik boksit yataklarının oluşumuyla ilişkisi. MTA Yerbilimleri ve Madencilik Dergisi **7**, 18–33 (2025)
145. Haude, H.: Stratigraphie und tektonik des südlichen Sultan Dağ (SW-Anatolien). Zeit. Deutsch. Geol. Ges, Hannover **123**, 411–421 (1972). https://doi.org/10.1127/zdgg/123/1972/411